

# Quantum Natural Stochastic Pairwise Coordinate Descent

Mohammad Aamir Sohail <sup>\*</sup>, Mohsen Heidari Khoozani <sup>†</sup>, and S. Sandeep Pradhan <sup>\*</sup>

<sup>\*</sup> Department of EECS, University of Michigan, Ann Arbor, USA

<sup>†</sup> Department of Computer Science, Indiana University, Bloomington, USA

<sup>\*</sup> mdaamir@umich.edu <sup>†</sup> mheidar@iu.edu <sup>\*</sup> pradhanv@umich.edu

## Abstract

Quantum machine learning through variational quantum algorithms (VQAs) has gained substantial attention in recent years. VQAs employ parameterized quantum circuits, which are typically optimized using gradient-based methods. However, these methods often exhibit sub-optimal convergence performance due to their dependence on Euclidean geometry. The quantum natural gradient descent (QNGD) optimization method, which considers the geometry of the quantum state space via a quantum information (Riemannian) metric tensor, provides a more effective optimization strategy. Despite its advantages, QNGD encounters notable challenges for learning from quantum data, including the no-cloning principle, which prohibits the replication of quantum data, state collapse, and the measurement postulate, which leads to the stochastic loss function. This paper introduces the quantum natural stochastic pairwise coordinate descent (2-QNSCD) optimization method. This method leverages the curved geometry of the quantum state space through a novel ensemble-based quantum information metric tensor, offering a more physically realizable optimization strategy for learning from quantum data. To improve computational efficiency and reduce sample complexity, we develop a highly sparse unbiased estimator of the novel metric tensor using a quantum circuit with gate complexity  $\Theta(1)$  times that of the parameterized quantum circuit and single-shot quantum measurements. Our approach avoids the need for multiple copies of quantum data, thus adhering to the no-cloning principle. We provide a detailed theoretical foundation for our optimization method, along with an exponential convergence analysis. Additionally, we validate the utility of our method through a series of numerical experiments.

## I. INTRODUCTION

The potential for quantum computers (QCs) to solve complex problems exponentially faster than classical computers promises revolutionary advancements in data analysis, optimization, and encryption [EFH<sup>+</sup>22], [Hwa03], [ZZWS17], [Sho94], [Gro96], [Sho99], [AJL06], [HHL09], [BCvD05]. With these rapid advancements in QC, there has been significant research interest in the development of quantum algorithms for applications involving quantum data (such as data generated by quantum many-body systems [Tas20] and quantum sensors [DRC17]). Examples of such applications include quantum anomaly detection [LR18], quantum

state discrimination [CWS<sup>+</sup>21], [SWL<sup>+</sup>17], quantum pattern matching [SC02], quantum data classification [SMMT<sup>+</sup>19], [DCH<sup>+</sup>21], and quantum sensor networks [XLZZ21], [HS10], [LCPLS13].

Toward this endeavor, substantial efforts have been made in designing quantum learning and optimization algorithms through a broad class of variational quantum algorithms (VQAs) [FN18], [MNKF18], [BBF<sup>+</sup>20], [SSP14], which include popular frameworks like the variational quantum eigensolver (VQE) [TCC<sup>+</sup>22], quantum neural networks (QNNs) [MVAF21], [GR20], and the quantum approximate optimization algorithm (QAOA) [FGG14]. These models involve parameterized quantum circuits (PQC) with tunable parameters that can be *learned* using quantum-classical optimization loops. Typically, gradient descent (GD) is used as a classical optimizer in VQAs due to its ease of implementation. However, it often suffers in terms of performance. Specifically, GD has a greater possibility of getting trapped at saddle points and may not converge to a local minimum [DPG<sup>+</sup>14]. GD strongly relies on Euclidean or  $\ell_2$  geometry within the parameter space [AD98], which poses a significant drawback because a notable distance between parameters (measured using Euclidean distance) may not necessarily have an equivalent influence on the underlying parameterized quantum states. This means that for two different sets of parameters with a large Euclidean distance, the corresponding parameterized quantum states may be indistinguishable. Therefore, it is preferable to measure the distance between parameterized quantum states and perform the steepest descent by considering the geometry of the space of these parametrized quantum states.

In light of this, quantum natural gradient descent (QNGD) [SIKC20] has been proposed as a more suitable optimization method alternative to GD. QNGD moves in the steepest direction with respect to the quantum information (Riemannian) metric tensor associated with the space of quantum states, and it remains invariant under any smooth and invertible re-parameterizations [Ama98], [Mar20]. Previous studies have shown that QNGD provides an advantage in optimizing quantum systems by taking optimization paths more aligned with the underlying geometric structure of quantum states, compared to other strategies [WGK20], [Yam19].

Despite these advantages, using QNGD presents notable challenges in learning from quantum data for the following reasons: (i) Probing (or measuring) a quantum state results in state collapse and produces a realization of a random process. This restricts access to the complete information about a quantum state. (ii) Stochasticity of quantum measurements results in the stochastic computation of the loss function. As a result, the precise estimation of gradients requires an exponential amount of measurements. (iii) In the case of a density matrix (or mixed state), the quantum information metric tensor reduces to the Bures metric tensor [LYLW20], [PS96], [Pet98], which relies on the spectral decomposition of the density matrix. Thus, evaluating the Bures metric tensor necessitates a full-state tomography of the density matrix, which in turn requires an exponential number of identical copies of the quantum state with the unknown density matrix. (iv) No-cloning theorem implies that an unknown quantum state cannot be replicated [WZ82]. This means

that a quantum state can only be measured once to extract any information. (v) Every iteration of QNGD requires evaluating the quantum information metric tensor, which has a cost that scales quadratically with the number of PQC parameters. These are further elaborated on in Section III.

To the best of our knowledge, QNGD has not been thoroughly explored due to these physical constraints in the context of quantum machine learning (QML) for quantum data. The majority of the prior works have focused on the following aspects: single-shot gradient estimation [HGS22], reducing the computational complexity of quantum information metric tensor, and improving methods for its estimation [GZCW21], [KB22], [vSK21]. Some of these works have primarily focused on finding the ground state energy of a quantum system using VQE. Moreover, there is no rigorous proof of the exponential convergence rate of QNGD in training a quantum learning model despite several experiments demonstrating faster convergence than GD.

In this work, we present a comprehensive solution to the problem of QML for quantum data in the framework of VQA. Our solution is based on a novel QNGD optimization method with a  $\Theta(1)$ -sample complexity per iteration, satisfying the aforementioned physical constraints and guaranteeing an exponential convergence rate. This approach aims to make QNGD practical and efficient for QML applications involving quantum data.

#### A. Motivation: Illustrative Example

Before we state our contributions and results, as a motivation for this work, we present an example that demonstrates the performance gain of QNGD over GD. Specifically, we illustrate that QNGD has the potential to escape saddle points, while GD tends to get trapped at those points.

We consider the problem of finding the ground state of a single-qubit Hamiltonian  $\mathcal{H} = \sigma_X$  using QNGD and GD, where  $\sigma_X$  is the Pauli  $X$  matrix. QNGD outperforms GD both in terms of convergence and the number of iterations as illustrated in Fig. 1. The energy landscape of the Hamiltonian as a function of parameters  $(\theta, \phi) \in [0, \pi) \times [\pi/2, 3\pi/2]$  of a pure state  $|\psi(\theta, \phi)\rangle$  is shown in Fig. 1(a). The corresponding contour plot with vector field of steepest descent direction in the Euclidean parameter space, i.e.,  $-\nabla \mathcal{L}(\theta, \phi)$  is shown in Fig. 1(d). The global minimum is marked as a red dot, and the saddle points are marked in black. Convergence for GD (blue) and QNGD (red) against the number of iterations for initial points in regions  $\mathcal{R}_1$  and  $\mathcal{R}_2$  are shown in Fig. 1(b) and (e), respectively. The region  $\mathcal{R}_1$  (two black lines) and  $\mathcal{R}_2$  (shaded in red) are shown in Fig. 1(c) and (f). The parameter trajectory taken by GD (blue) and QNGD (red) starting from initial points are also shown here. It can be noted from Fig. 1(b) and (c) that GD slows down near saddle points and gets trapped at those points, while QNGD navigates the landscape successfully by considering the underlying geometry of the space of pure quantum states to reach the global minimum. Moreover, from Fig. 1(e) and (f), it can be observed that QNGD (blue) finds the minimum more efficiently, avoiding the flat boundary regions that attract GD (red). The region  $(\mathcal{R}_1 \cup \mathcal{R}_2)$  is the set of initial parameters for which GD

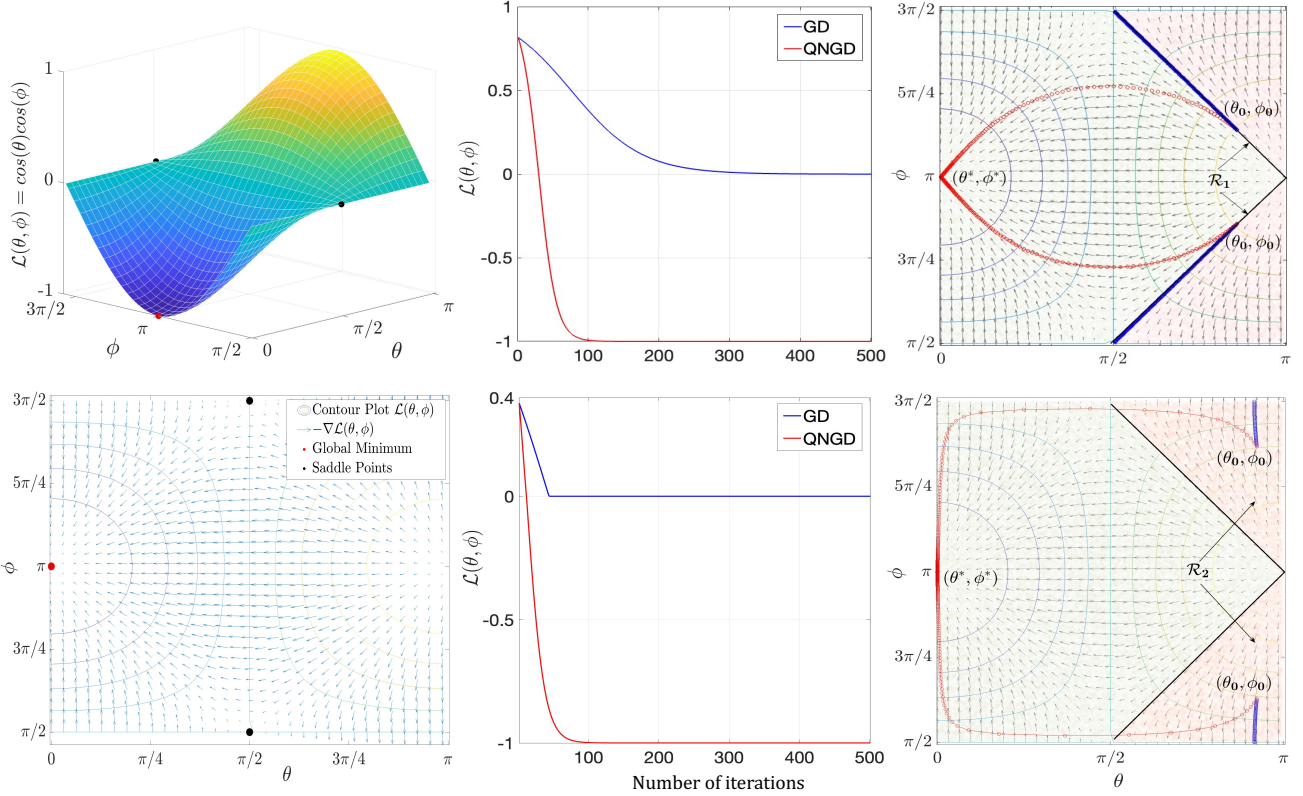


Figure 1: Comparison of GD and QNGD in finding the ground state of a single-qubit Hamiltonian: QNGD escapes saddle points and reaches the global minimum more efficiently than GD.

fails to converge, and the green-shaded region is the set of initial parameters for which GD converges. On the other hand, QNGD converges for every initial parameter in the domain. The example is further detailed in Appendix A.

### B. Contribution and Results

In this work, we present quantum natural stochastic pairwise coordinate descent (2-QNSCD) optimization method, where each iteration requires only a constant number of training quantum samples. We summarize the key contributions by informally stating the main results below. Let  $\mathcal{L}(\boldsymbol{\theta})$  be a loss function associated with a PQC described by a parameterized unitary  $U(\boldsymbol{\theta})$ , followed by a measurement (POVM)  $\{\Lambda_y\}_{y \in \mathcal{Y}}$ . The unitary  $U(\boldsymbol{\theta})$  acts on an input ensemble of quantum states  $\{(Q_X(x), |\phi_x\rangle)\}_{x \in \mathcal{X}}$  with  $\rho$  being the corresponding density matrix, as described in Section II.

- We present a new quantum information metric tensor for an ensemble of pure states, namely, ensemble-based quantum Fisher information metric (E-QFIM), denoted as  $\mathcal{F}^{\mathcal{E}}$ . This new ensemble-based metric can be efficiently estimated without the need for full-state tomography of the density matrix corresponding to the ensemble of pure states as needed in the case of the Bures metric tensor. This circumvents the no-cloning

theorem by not demanding copies of a density matrix. We derive the following characterization stated below (see Theorem 1 for the formal statement) by constructing a new distance measure on ensembles using ensemble fidelity, which serves as a lower bound to the Uhlmann fidelity between the density matrices of the corresponding ensembles (see Section IV-A).

**Theorem I.1** (informal). *For a given PQC and an input density matrix  $\rho$ , the matrix elements of the E-QFIM are given as:*

$$\mathcal{F}_{(i,j)}^{\mathcal{E}}(\boldsymbol{\theta}) := \text{Re}\{\text{Tr}(\Upsilon_i(\boldsymbol{\theta})\Upsilon_j(\boldsymbol{\theta})\rho) - \text{Tr}(\Upsilon_i(\boldsymbol{\theta})\rho)\text{Tr}(\Upsilon_j(\boldsymbol{\theta})\rho)\}, \quad (1)$$

where  $\Upsilon_i$  is a Hermitian matrix defined as:

$$\Upsilon_i := -i \left( \frac{\partial}{\partial \theta_i} U^\dagger(\boldsymbol{\theta}) \right) U(\boldsymbol{\theta}) = i U^\dagger(\boldsymbol{\theta}) \left( \frac{\partial}{\partial \theta_i} U(\boldsymbol{\theta}) \right).$$

- We provide a highly sparse unbiased estimator of E-QFIM, denoted as  $\bar{\mathbf{Z}}$ , which incorporates the underlying geometry of the space of quantum states corresponding to only a pair of random parameter coordinates. This is summarized in the theorem below (see Theorem 2 for the formal statement).

**Theorem I.2** (Unbiased Estimation of  $\mathcal{F}^{\mathcal{E}}$  (informal)). *There exists an algorithm (Algorithm 1 in Section IV-B1) that takes  $\Theta(1)$  training quantum data to provide an unbiased estimation of the metric, i.e.,  $\mathbb{E}[\bar{\mathbf{Z}}] = \mathcal{F}^{\mathcal{E}}$ , where the expectation is over the random pair of coordinates chosen at every iteration, input quantum state, and the outcome of quantum measurements.*

$\bar{\mathbf{Z}}$  mitigates the aforementioned quadratic computational cost associated with the number of PQC parameters and ensures that the computational cost remains constant as the number of PQC parameters increases. Additionally, we present quantum circuits that construct this estimator using a constant number of training quantum data and single-shot quantum measurements, thereby reducing the need for repeated measurements. The circuit does not require any additional ancilla qubits, and its gate complexity is  $\Theta(1)$  times that of the PQC.

- We present a novel  $\Theta(1)$ -sample complexity (per iteration) QNGD optimization method, namely, quantum natural stochastic pairwise coordinate descent (2-QNSCD). At each iteration, 2-QNSCD uses a constant amount of training quantum data without requiring identical copies and updates only two parameters using the following update rule:

$$\boldsymbol{\theta}^{(t+1)} = \boldsymbol{\theta}^{(t)} - \eta_t |\bar{\mathbf{Z}}^t(i, j)|^{-1} \mathbf{g}^t(i, j), \quad (2)$$

where  $(i, j)$  is a pair of coordinates chosen randomly at every iteration,  $\eta_t$  is a learning rate, and  $\mathbf{g}^t$  is an unbiased estimator of the gradient  $\nabla \mathcal{L}$ . We demonstrate the data efficiency of 2-QNSCD as it does not need data replication to deal with the stochastic loss function associated with state collapse after performing a quantum measurement. This addresses the challenge of accessing complete information about a quantum state

to evaluate the loss function (see Sections IV-B).

- We provide a convergence analysis of our 2-QNSCD optimization method under a mild assumption on the loss function and without the need for quantum data replication. The following theorem summarizes the exponential convergence rate (see Theorem 3 for the formal statement).

**Theorem I.3** (Convergence of 2-QNSCD (informal)). *Under the mild assumption, 2-QNSCD with a fixed learning rate  $\eta = \beta/L_2$  achieves a global exponential convergence rate, given by,*

$$\mathbb{E}[\mathcal{L}(\boldsymbol{\theta}^{(t)}) - \mathcal{L}(\boldsymbol{\theta}^*)] \leq \left(1 - \frac{8\bar{\mu}\beta}{c^3 L_2}\right)^t (\mathcal{L}(\boldsymbol{\theta}^{(0)}) - \mathcal{L}(\boldsymbol{\theta}^*)) + \frac{c}{8\bar{\mu}}\alpha^2\beta^2, \quad (3)$$

where  $\boldsymbol{\theta}^*$  is the global optimizer for  $\mathcal{L}(\boldsymbol{\theta})$ ,  $\alpha$  is a function of the moments of estimators,  $\beta$  is a regularization parameter,  $\bar{\mu}$  and  $L_2$  are constants characterized by the assumptions on  $\mathcal{L}(\boldsymbol{\theta})$ .

- We support our theoretical findings with experimental results highlighting 2-QNSCD's scalability, data efficiency, and faster convergence rate. Our evaluations, using multiple PQCs, demonstrate faster convergence. In contrast, the corresponding GD method with  $\Theta(1)$ -sample complexity per iteration potentially converges to a local minimum or gets stuck at saddle points (see Section V).
- In the pursuit of the 2-QNSCD convergence analysis, we also characterize a sufficient condition required for the exponential convergence rate of QNGD (see Theorem 4), assuming complete access to the metric tensor and the gradient. Specifically, we introduce the *quadratic geometric information* (QGI) inequality (see Definition 4), which serves as a more general metric-dependent criterion compared to the Polyak-Łojasiewicz (PL) inequality<sup>1</sup> [Pol63] and ensures an exponentially faster rate of convergence (see Section VI).

### C. Roadmap of the Paper

The paper is organized as follows: In Section II, we discuss our PQC architecture and formulate the quantum learning model. Section III provides background on QNGD and a gist of related works. In Section IV, we present our main results (Theorems 1,2, and 3) with regard to 2-QNSCD, and leaving proofs for Appendices. Section V describes our experiments and observed results. For completeness, we provide the convergence analysis of the QNGD method with complete access to the metric tensor and the gradient in Section VI.

**Notations:** We use  $[c] := \{1, 2, \dots, c\}$ . The indicator random variable is denoted as  $\mathbb{1}_{\{\cdot\}}$ . Vectors are represented in boldface, such as  $\boldsymbol{\theta}$ , and matrices are denoted by uppercase boldface letters, such as  $\mathbf{Z}$ . In this paper,  $\|\cdot\|$  denotes the  $\ell_2$  (Euclidean) norm for vectors and the spectral norm for matrices unless otherwise specified. For a given matrix  $\mathbf{Z}$ , we denote the element of  $\mathbf{Z}$  in the  $i^{\text{th}}$  row and  $j^{\text{th}}$  column as  $\mathbf{Z}_{(i,j)}$ , and  $\mathbf{Z}_{[i,j]}$  denotes

<sup>1</sup>If a loss function satisfies the PL inequality, GD achieves an exponential convergence rate to the global minimum. It was first shown by Polyak in 1963; for more details, please refer to [KNS16], [Pol63].

the  $2 \times 2$  submatrix of  $\mathbf{Z}$  formed by selecting the  $i^{\text{th}}$  and  $j^{\text{th}}$  rows and columns. To denote derivatives with respect to the  $i^{\text{th}}$  coordinate of a vector  $\boldsymbol{\theta}$ , we use  $\partial_i := \frac{\partial}{\partial \theta_i}$ . We denote the Hilbert space of  $d$ -qubits as  $\mathcal{H}^d$ . For a given pure quantum state  $|\phi\rangle$ , the corresponding density matrix is denoted as  $\Phi := |\phi\rangle\langle\phi|$ . To represent a series of quantum operations, we introduce the following shorthand notation:  $W_{[a:b]} := W_a W_{a+1} \cdots W_b$ , when  $a \leq b$  and  $W_{[a:b]} := W_a W_{a-1} \cdots W_b$ , when  $a > b$ .

## II. PROBLEM SETUP

In this section, we discuss our PQC architecture and formalize the QML model involving quantum data under the supervised learning framework.

**PQC architecture:** We consider standard multi-layered parameterized unitary operators acting on the Hilbert space  $\mathcal{H}^d$  as our PQC to train the QL model. Each layer is composed of a parameterized unitary operator, denoted as  $U_a(\boldsymbol{\theta}_a)$ , followed by a non-parameterized (fixed) unitary operator, denoted as  $V_a$ , where  $a$  is the layer index, and  $\boldsymbol{\theta}_a \in [0, 2\pi]^d$  is a parameter vector corresponding to the layer  $a$ . For simplicity of exposition, the parameterized unitaries consist of tensor products of single-qubit Pauli rotations, i.e.,  $U_a(\boldsymbol{\theta}_a) := \bigotimes_{p=1}^d R_{\sigma_p^a}(\boldsymbol{\theta}_{(a,p)})$ , where  $p$  denotes the qubit index,  $\boldsymbol{\theta}_{(a,p)} \in [0, 2\pi]$  is the parameter corresponding to the  $(a^{\text{th}}$  layer,  $p^{\text{th}}$  qubit) unitary operator,  $\sigma_p^a$  are Pauli operators, and  $R_{\sigma_p^a}(\boldsymbol{\theta}_{(a,p)}) := \exp(-i\boldsymbol{\theta}_{(a,p)}\sigma_p^a/2)$  is the rotation operator corresponding to  $\sigma_p^a$ . Thus, mathematically, our PQC with  $L$  layers is a parameterized unitary operator, defined as:

$$U(\boldsymbol{\theta}) := V_L U_L(\boldsymbol{\theta}_L) \cdots V_2 U_2(\boldsymbol{\theta}_2) V_1 U_1(\boldsymbol{\theta}_1), \quad (4)$$

where  $\boldsymbol{\theta} \in [0, 2\pi]^c$  represents a vector comprising all the parameters across each layer and  $c = dL$  is the number of PQC parameters. For conciseness, we use the shorthand notation  $W_a(\boldsymbol{\theta}_a) := V_a U_a(\boldsymbol{\theta}_a)$  throughout the rest of the paper.

**Quantum Learning Model:** We focus on a supervised learning model with quantum data labeled by a classical variable. Consider an unknown but fixed probability distribution  $Q_{XY}$  on  $\mathcal{X} \times \mathcal{Y}$ , where  $\mathcal{X}$  and  $\mathcal{Y}$  are finite sets. The feature set is an ensemble of pure quantum states  $\mathcal{E} := \{(Q_X(x), |\phi_x\rangle)\}$ , where  $\rho := \sum_{x \in \mathcal{X}} Q_X(x) |\phi_x\rangle\langle\phi_x|$  represents the corresponding density matrix, and  $\mathcal{Y}$  represents the set of all possible classical labels.

With this setup, consider the PQC  $U(\boldsymbol{\theta})$  as discussed above. As a training set, we are given  $n$  independent and identically distributed (i.i.d.) samples  $\{(|\phi_{x_i}\rangle, y_i)\}_{i \in [n]}$ , where  $(x_i, y_i)$  are randomly generated according to  $Q_{XY}$ . A supervised quantum classification learning algorithm processes the training samples using  $U(\boldsymbol{\theta})$ , followed by a quantum measurement characterized via a POVM (positive operator-valued measure)  $\Lambda := \{\Lambda_{\hat{y}} \geq 0 : \sum_{\hat{y} \in \mathcal{Y}} \Lambda_{\hat{y}} = I\}$  (referred to as predictor) to predict the labels of unseen samples. The goal of the learning algorithm is to find an optimal  $\boldsymbol{\theta}^*$  that ensures the predicted label closely matches the given training labels for each training quantum sample.

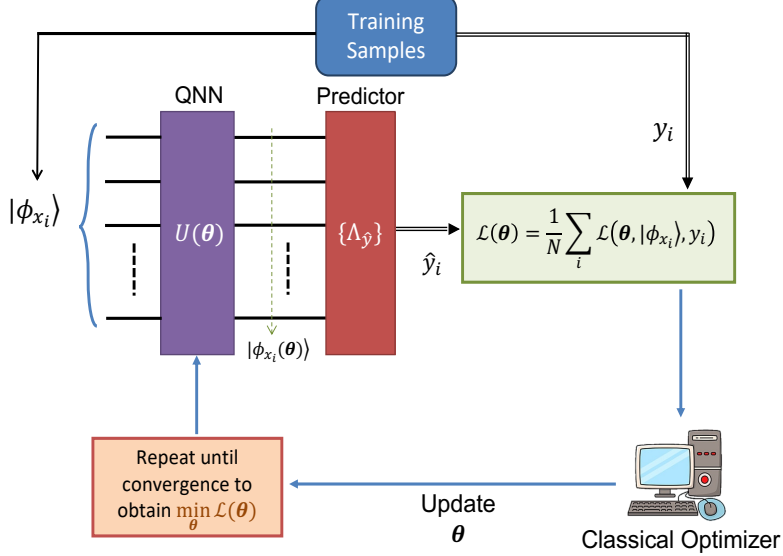


Figure 2: Quantum Learning Model

**Loss function:** Given a sample  $|\phi_x\rangle$ , the model generates a label  $\hat{y}$  as the output of the measurement according to a conditional probability distribution, as determined by Born's rule:

$$P_{Y|X}(\hat{y}||\phi_x, \theta) = \text{Tr}\{\Lambda_{\hat{y}} U(\theta) \Phi_x U^\dagger(\theta)\}. \quad (5)$$

Let  $\hat{Y}$  denote the corresponding random variable. To measure the incurred prediction loss, we employ a loss function  $\ell : \mathcal{Y} \times \mathcal{Y} \rightarrow [0, \infty)$ , for example, 0-1 loss, absolute loss, and squared loss. Then, conditioned on a fixed sample  $(|\phi_x\rangle, y)$ , the per-sample expected loss taken with respect to  $\hat{Y}$  is expressed as:

$$\mathcal{L}(\theta, |\phi_x\rangle, y) := \mathbb{E}_{P_{Y|X}}[\ell(y, \hat{Y})] = \sum_{\hat{y} \in \mathcal{Y}} \ell(y, \hat{y}) \text{Tr}\{\Lambda_{\hat{y}} U(\theta) \Phi_x U^\dagger(\theta)\}. \quad (6)$$

After taking the expectation over the sample's distribution, we get the incurred expected loss as a function of  $\theta$ :  $\mathcal{L}(\theta) := \mathbb{E}_{Q_{XY}}[\mathcal{L}(\theta, |\phi_X\rangle, Y)]$ . Since the underlying distribution  $Q_{XY}$  is unknown, directly minimizing the expected loss is not feasible. Consequently, given the sample set  $\{(|\phi_{x_i}\rangle, y_i)\}_{i \in [n]}$ , we aim to minimize the incurred average per-sample expected loss:

$$\bar{\mathcal{L}}(\theta) := \frac{1}{n} \sum_{i=1}^n \mathcal{L}(\theta, |\phi_{x_i}\rangle, y_i) = \frac{1}{n} \sum_{i=1}^n \sum_{\hat{y} \in \mathcal{Y}} \ell(y_i, \hat{y}) \text{Tr}\{\Lambda_{\hat{y}} U(\theta) \Phi_{x_i} U^\dagger(\theta)\}. \quad (7)$$

The quantum learning model is illustrated in Fig. 2.

### III. BACKGROUND AND RELATED WORK

Recent demonstrations, such as the parameter shift rule and finite differencing [MNKF18], [SBG<sup>+</sup>18], [HN21], [KMT<sup>+</sup>17], [BC21], showcase the ability to compute gradients for quantum circuits by estimating the loss

function using multiple identical copies of a quantum state<sup>2</sup>. Therefore, the stochastic gradient descent (SGD) method can be considered to train the quantum learning model via an update rule of the form:

$$\boldsymbol{\theta}^{(t+1)} = \boldsymbol{\theta}^{(t)} - \eta_t \nabla \mathcal{L}(\boldsymbol{\theta}^{(t)}, |\phi_{x_t}\rangle, y_t), \quad (8)$$

where  $\eta_t$  is the learning rate at iteration  $t$ . Further, to mitigate the need for multiple identical copies of a quantum state, [HGS22] proposed a single-shot gradient estimations method, namely, a randomized quantum stochastic gradient descent (RQSGD) optimization technique. Nevertheless, as mentioned in the introduction, GD is inefficient at handling saddle points. These points are often surrounded by a plateau of small curvature, causing the gradient to diminish rapidly and significantly slowing down the training process. To address this, one may consider a second-order optimization method, such as the Newton method [BV04], which utilizes the Hessian of the loss function. The update step of the Newton method replaces the gradient by multiplying the gradient with the inverse of the Hessian matrix. However, this does not address saddle points satisfactorily, and instead, saddle points become attractive under Newton dynamics, as argued in [DPG<sup>+</sup>14, Section 4]. In 1998, Amari *et al.* [Ama98] proposed the concept of natural gradient descent (NGD), where the Hessian is replaced with Fisher information. NGD has been shown to effectively address certain saddle point structures, as argued by [RSA98], [IPO03]. Furthermore, NGD is invariant under arbitrary smooth and invertible reparameterizations, whereas Newton method is invariant only under affine coordinate transformation [Ama98], [Mar20].

In a similar spirit, QNGD [SIKC20] has been proposed as an optimization method based on the information geometry of the space of quantum states, which uses a quantum information (Riemannian) metric tensor as

$$\boldsymbol{\theta}^{(t+1)} = \boldsymbol{\theta}^{(t)} - \eta_t \mathsf{F}(\boldsymbol{\theta}^{(t)})^{-1} \nabla \mathcal{L}(\boldsymbol{\theta}^{(t)}, |\phi_{x_t}\rangle, y_t), \quad (9)$$

where  $\mathsf{F}(\boldsymbol{\theta}^{(t)})$  denotes quantum information metric tensor. In (9),  $\mathsf{F}^{-1} \nabla \mathcal{L}$  is the steepest direction in the space of quantum states. Essentially, here, each optimization step computes the steepest descent direction of the per-sample expected loss around the local value of  $\boldsymbol{\theta}^{(t)}$  on the space of quantum states and updates  $(\boldsymbol{\theta}^{(t)} \rightarrow \boldsymbol{\theta}^{(t+1)})$  accordingly. A number of studies have demonstrated the performance gains achieved by QNGD over GD. For instance, [WGK20] shows that QNGD provides an advantage for optimizing quantum systems by taking an optimal parameters path compared to other optimization strategies. For more details, we suggest [SIKC20], [Yam19], [TWXL23], [WXW<sup>+</sup>23], [QZT23], [Mey21], [KW23].

In the literature, the quantum information metric tensor is derived using a suitably defined distance measure,

<sup>2</sup>Note that, unlike classical learning, in quantum domain exact computation of loss function is not possible because quantum states  $|\phi_x\rangle$  are unknown, i.e., we do not have complete knowledge of  $|\phi_x\rangle$ . If we perform measurement on a quantum state to access information, it will result in a state collapse. Therefore, one can only estimate the loss function using multiple identical copies of a quantum state.

denoted as  $d(\boldsymbol{\theta}, \boldsymbol{\theta}')$ , in the space of quantum states. The squared infinitesimal distance can be expressed in terms of quantum information metric tensor (Taylor series around  $d\boldsymbol{\theta} = 0$ ) as:

$$ds^2 := d^2(\boldsymbol{\theta}, \boldsymbol{\theta} + d\boldsymbol{\theta}) \approx \sum_{i,j} \mathsf{F}(\boldsymbol{\theta})_{(i,j)} d\boldsymbol{\theta}_i d\boldsymbol{\theta}_j,$$

where the first-order term goes to zero as  $d\boldsymbol{\theta} = 0$  corresponds to a minimum<sup>3</sup>, and the second-order term is the first non-zero contribution of the Taylor series expansion around  $d\boldsymbol{\theta} = 0$ . In the case of pure states, the distance measure is defined using the fidelity between pure states as

$$d^2(|\phi(\boldsymbol{\theta})\rangle, |\phi(\boldsymbol{\theta}')\rangle) = (2 - 2\sqrt{f_\phi(\boldsymbol{\theta}, \boldsymbol{\theta}')}), \quad (10)$$

where  $f_\phi(\boldsymbol{\theta}, \boldsymbol{\theta}') := |\langle\phi(\boldsymbol{\theta})|\phi(\boldsymbol{\theta}')\rangle|^2$ , and  $\mathsf{F}$  reduces to the Fubini-Study metric tensor  $\mathsf{F}^\phi$  (see Definition 1 below), as demonstrated by Petz et al. [PS96], [Pet98].

**Definition 1** (Fubini-Study Metric Tensor). *The Fubini-Study metric tensor, denoted as  $\mathsf{F}^\phi$ , is a Riemannian metric tensor defined on the complex projective space  $\mathbf{CP}^n$ , which is the space of pure states with global phase factored out. For a given parameterized pure state  $|\phi(\boldsymbol{\theta})\rangle$ , the entries of  $\mathsf{F}^\phi$  are given as:*

$$\mathsf{F}_{(i,j)}^\phi(\boldsymbol{\theta}) = \text{Re}\{\langle\partial_i\phi(\boldsymbol{\theta})|\partial_j\phi(\boldsymbol{\theta})\rangle - \langle\partial_i\phi(\boldsymbol{\theta})|\phi(\boldsymbol{\theta})\rangle\langle\phi(\boldsymbol{\theta})|\partial_j\phi(\boldsymbol{\theta})\rangle\},$$

where  $i, j \in [c]$  and  $c$  is the number of parameters. It measures the effect of changing parameters on the underlying parameterized pure state.

For density matrices,  $\mathsf{F}$  reduces to the Bures metric tensor  $\mathsf{F}^\rho$  (see Definition 2 below) [Bur69], [BC94], [LYLW20], [LXSW14] using Bures distance [NC10] between density matrices given as

$$d_B^2(\rho(\boldsymbol{\theta}), \rho(\boldsymbol{\theta}')) = (2 - 2\sqrt{f_\rho(\boldsymbol{\theta}, \boldsymbol{\theta}')}), \quad (11)$$

where  $f_\rho(\boldsymbol{\theta}, \boldsymbol{\theta}') := (\text{Tr}\{(\sqrt{\rho(\boldsymbol{\theta})}\rho(\boldsymbol{\theta}')\sqrt{\rho(\boldsymbol{\theta})})^{1/2}\})^2$  is the Uhlmann fidelity [Wil13] and  $\rho(\boldsymbol{\theta})$  is a parameterized density matrix.

**Definition 2** (Bures Metric Tensor). *The Bures metric tensor, denoted as  $\mathsf{F}^\rho$ , is a Riemannian metric tensor defined on the space of density matrices. For a given parameterized density matrix  $\rho(\boldsymbol{\theta})$ , the entries of  $\mathsf{F}^\rho$  are given as*

$$\mathsf{F}_{(i,j)}^\rho := \sum_k \frac{1}{4} \frac{(\partial_i \lambda_k)(\partial_j \lambda_k)}{\lambda_k} + \sum_k \lambda_k \text{Re}\{\langle\partial_i \lambda_k|\partial_j \lambda_k\rangle\} - \sum_{k_1, k_2} \frac{2\lambda_{k_1}\lambda_{k_2}}{\lambda_{k_1} + \lambda_{k_2}} \text{Re}\{\langle\partial_i \lambda_{k_1}|\lambda_{k_2}\rangle\langle\lambda_{k_2}|\partial_j \lambda_{k_1}\rangle\},$$

where  $i, j \in [c]$ ,  $c$  is the number of parameters, and  $\rho(\boldsymbol{\theta}) = \sum_k \lambda_k |\lambda_k\rangle\langle\lambda_k|$  is the spectral decomposition of  $\rho(\boldsymbol{\theta})$  with parameterized eigenvalues  $\lambda_k (\neq 0)$  and parameterized eigenvectors  $|\lambda_k\rangle$ .

<sup>3</sup>A distance measure  $d(\boldsymbol{\theta}, \boldsymbol{\theta}')$  is non-negative and equals zero for identical parameters, i.e.,  $d(\boldsymbol{\theta}, \boldsymbol{\theta}) = 0$  is a minimum.

Unfortunately, none of these information metric tensors can be efficiently used in QNGD methods for learning from quantum data due to the following reasons. The Fubini-Study metric tensor is defined only for pure states, and the feature set in the model is an ensemble of pure states. Therefore, one may consider the Bures metric tensor, defined on the density matrix of the feature set. However, computing the Bures metric tensor is much more involved and requires a full tomography of the feature density matrix to access the eigenvalue and eigenvectors of the density matrix to compute  $\mathsf{F}^\rho$ , requiring an exponential number of identical copies of  $\rho$ . Precisely, to measure a  $d$ -qubit quantum state  $\rho$  of rank  $r$  using quantum state tomography with  $\varepsilon$ -accuracy in terms of trace distance, requires  $O(2^d r^2 / \varepsilon^2)$  copies [FGL12], [GLF<sup>+</sup>10], [HHJ<sup>+</sup>16]. Alternatively, many approximation methods have been proposed, including a pure-state approximation of mixed-quantum state [KB22], [Koc21a], [Koc21b] and truncated  $\mathsf{F}^\rho$  [SCBC21]. In these works, the authors approximated the Bures metric tensor to a few dominant eigenvectors of  $\rho$  with an additional error, which decreases exponentially in the number of copies of  $\rho$ . For more information refer to [BCSC22], [RBMV21], [VRJ<sup>+</sup>23]. While these works offer various approaches, they share a crucial drawback: requiring an exponentially increasing number of copies of  $\rho$  to achieve negligible error in metric estimation.

Furthermore, QNGD requires evaluation of the quantum information metric tensor at each iteration, which can be computationally intensive. This becomes particularly demanding when dealing with a large number of PQC parameters as computing  $\mathsf{F}$  requires evaluating  $O(c^2)$  terms. Various techniques have been proposed to mitigate this computational cost, reducing it to linear complexity, such as block-diagonal approximation [SIKC20] and second-order simultaneous perturbation methods [GZCW21] for the Fubini-Study metric tensor. However, it is important to note that such approximations may not precisely capture parameter correlations. Therefore, QNGD can not perform well in situations where parameters are highly correlated. In addition, computing  $\mathsf{F}$  (exact or approximation) involves calculating fidelity between two quantum states, which can be done using quantum circuits such as the SWAP test [BCWDW01], the Hadamard test [CEMM98], and the compute-uncompute method [HCT<sup>+</sup>19]. However, these techniques require an exponential number of measurements for the estimation of fidelities associated with the metric tensor. Precisely, pure state fidelity is approximated with up to  $\varepsilon$  error by performing  $O(1/\varepsilon^2)$  measurements [WIWL22], where  $\varepsilon \in (0, 1)$ .

To overcome these challenges, we introduce a novel ensemble-based quantum information metric tensor, referred to as E-QFIM  $\mathcal{F}^E$ . This metric is based on a covariance structure, and it is designed to be efficiently estimated without any bias and quantum state replication. Furthermore, our proposed 2-QNSCD optimization method only requires the underlying geometry of the space of quantum states corresponding to a pair of parameter coordinates at each iteration. This results in the construction of highly sparse E-QFIM estimators using only a constant number of training quantum samples at each iteration.

#### IV. MAIN RESULTS

In this section, we present the main findings of our work. We begin by introducing the concept of E-QFIM. Firstly, we establish the framework for constructing E-QFIM and then proceed to derive the E-QFIM for our PQC model (discussed in Section II). Subsequently, we will introduce our 2-QNSCD optimization method. Following this, we move on to creating unbiased estimators of the E-QFIM and the gradient of the loss function. Finally, we conclude the section with a convergence analysis of 2-QNSCD.

##### A. Ensemble Quantum Fisher Information Metric (E-QFIM)

For a given ensemble of quantum states  $\mathcal{E} := \{Q_X(x), |\phi_x\rangle\}_{x \in \mathcal{X}}$ , define parameterized ensemble  $\mathcal{E}(\boldsymbol{\theta}) := \{Q_X(x), |\phi_x(\boldsymbol{\theta})\rangle\}_{x \in \mathcal{X}}$  with corresponding density matrix  $\rho(\boldsymbol{\theta}) := \sum_x Q_X(x) |\phi_x(\boldsymbol{\theta})\rangle \langle \phi_x(\boldsymbol{\theta})|$ , where  $|\phi_x(\boldsymbol{\theta})\rangle := U(\boldsymbol{\theta}) |\phi_x\rangle$  and  $U(\boldsymbol{\theta})$  is a unitary operator describing the PQC model.

We begin by outlining the central idea that gives us the ensemble-based metric tensor. We consider deriving a lower bound on the Uhlmann fidelity, ensuring that the resulting expression avoids any use of density matrix and can be calculated solely using the ensemble representation. To this end, consider the following inequalities:

$$\begin{aligned} f_\rho(\boldsymbol{\theta}, \boldsymbol{\theta}') &\geq \sum_x Q_X(x) f_{\phi_x}(\boldsymbol{\theta}, \boldsymbol{\theta}') \\ &= \sum_x Q_X(x) |\langle \phi_x(\boldsymbol{\theta}) | \phi_x(\boldsymbol{\theta}') \rangle|^2 \geq \left| \sum_x Q_X(x) \langle \phi_x(\boldsymbol{\theta}) | \phi_x(\boldsymbol{\theta}') \rangle \right|^2, \end{aligned} \quad (12)$$

where the first and second inequalities follow from the joint concavity of Uhlmann fidelity [Wil13, Ch.9] and Jensen's inequality, respectively. It can be observed that the lower bound expression above can be described using only the ensemble of pure states.

Now, to derive E-QFIM, we select the lower bound expression of (12) as a measure of closeness between ensembles of quantum states. We define *ensemble fidelity* between two ensembles of pure states characterized by parameters  $\boldsymbol{\theta}$  and  $\boldsymbol{\theta}'$  as

$$f_{\mathcal{E}}(\boldsymbol{\theta}, \boldsymbol{\theta}') := \left| \sum_{x \in \mathcal{X}} Q_X(x) \langle \phi_x(\boldsymbol{\theta}) | \phi_x(\boldsymbol{\theta}') \rangle \right|^2. \quad (13)$$

Subsequently, define a distance measure between ensembles of quantum states using (13) as follows:

$$d_E(\mathcal{E}(\boldsymbol{\theta}), \mathcal{E}(\boldsymbol{\theta}')) := (2 - 2\sqrt{f_{\mathcal{E}}(\boldsymbol{\theta}, \boldsymbol{\theta}')} )^{1/2}. \quad (14)$$

Using (12), it can be easily observed that (14) serves as an upper bound to the Bures distance. The ensemble distance measure is useful as a measure of the distinguishability of two ensembles  $\mathcal{E}(\boldsymbol{\theta})$  and  $\mathcal{E}(\boldsymbol{\theta}')$  because it is non-negative and equals zero if and only if every corresponding quantum state within  $\mathcal{E}(\boldsymbol{\theta})$  and  $\mathcal{E}(\boldsymbol{\theta}')$  is

essentially the same, i.e., differing solely by a constant global phase:  $|\phi_x(\boldsymbol{\theta}')\rangle = e^{i\delta} |\phi_x(\boldsymbol{\theta})\rangle$  for all  $x \in \mathcal{X}$ , where  $\delta \in [0, 2\pi]$ . This can be easily shown by considering the following inequalities:

$$\left| \sum_{x \in \mathcal{X}} Q_X(x) \langle \phi_x(\boldsymbol{\theta}) | \phi_x(\boldsymbol{\theta}') \rangle \right| \stackrel{a}{\leq} \sum_{x \in \mathcal{X}} Q_X(x) |\langle \phi_x(\boldsymbol{\theta}) | \phi_x(\boldsymbol{\theta}') \rangle| \stackrel{b}{\leq} \sum_x Q_X(x) = 1,$$

where (a) and (b) follows from Jensen's inequality and Cauchy–Schwarz inequality, respectively. Note that the first equality holds if and only if  $\langle \phi_x(\boldsymbol{\theta}) | \phi_x(\boldsymbol{\theta}') \rangle = r_x e^{i\delta}$  for all  $x \in \mathcal{X}$  and second equality holds if and only if  $|\phi_x(\boldsymbol{\theta}')\rangle = e^{i\delta_x} |\phi_x(\boldsymbol{\theta})\rangle$  for all  $x \in \mathcal{X}$ , where  $r_x \geq 0$ , and  $\delta, \delta_x \in [0, 2\pi]$ . Furthermore, we show in Appendix B that the distance measure  $d_E$  is monotonic, i.e., it does not increase under the action of any quantum channel (CPTP map [Wil13]).

Now, in order to understand how a change in the parameter  $\boldsymbol{\theta}$  affects the underlying ensemble, we examine how a slight perturbation of the parameter  $(\boldsymbol{\theta} + d\boldsymbol{\theta})$  reflects in the ensemble distance. We develop this by analyzing ensemble distance between two infinitesimally close ensembles using the Taylor series expansion around  $d\boldsymbol{\theta} = 0$  (see [SZ03], [LYLW20], [Mey21]). Noting the simple fact that the ensemble distance measure achieves its minimum for  $d\boldsymbol{\theta} = 0$ , i.e.,  $d_E(\mathcal{E}(\boldsymbol{\theta}), \mathcal{E}(\boldsymbol{\theta})) = 0$ , we infer that the first-order contribution vanishes around the minimum, and the second-order term will be the first contribution of the Taylor series expansion. The squared infinitesimal ensemble distance is expressed as:

$$ds^2 := d_E^2(\mathcal{E}(\boldsymbol{\theta}), \mathcal{E}(\boldsymbol{\theta} + d\boldsymbol{\theta})) = d\boldsymbol{\theta}^\top \mathcal{F}^{\mathcal{E}}(\boldsymbol{\theta}) d\boldsymbol{\theta} + O(\|d\boldsymbol{\theta}\|^3),$$

where we refer to  $\mathcal{F}^{\mathcal{E}}(\boldsymbol{\theta})$  as E-QFIM, whose entries are given as,

$$\mathcal{F}_{(a_p, b_q)}^{\mathcal{E}}(\boldsymbol{\theta}) = \frac{1}{2} \frac{\partial^2}{\partial d\boldsymbol{\theta}_{(a,p)} \partial d\boldsymbol{\theta}_{(b,q)}} d_E^2(\boldsymbol{\theta}, \boldsymbol{\theta} + d\boldsymbol{\theta}) \Big|_{d\boldsymbol{\theta}=0}.$$

Here, we use the short-hand notation  $a_p := (a, p)$ . The information metric  $\mathcal{F}^{\mathcal{E}}(\boldsymbol{\theta})$  essentially encapsulates all the information about the local vicinity of  $\boldsymbol{\theta}$ , measured by  $d_E$  in the space of quantum states. The E-QFIM can be calculated by the following theorem:

**Theorem 1.** *For a given unitary operator  $U(\boldsymbol{\theta})$  and ensemble  $\mathcal{E} = \{(Q_X(x), |\phi_x\rangle)\}$ , the elements of ensemble quantum Fisher information metric (E-QFIM) are given as:*

$$\mathcal{F}_{(a_p, b_q)}^{\mathcal{E}}(\boldsymbol{\theta}) := \text{Re} \{ \text{Tr}(\Upsilon_{(a,p)}(\boldsymbol{\theta}) \Upsilon_{(b,q)}(\boldsymbol{\theta}) \rho) - \text{Tr}(\Upsilon_{(a,p)}(\boldsymbol{\theta}) \rho) \text{Tr}(\Upsilon_{(b,q)}(\boldsymbol{\theta}) \rho) \}, \quad (15)$$

where  $\rho := \sum_{x \in \mathcal{X}} Q_X(x) |\phi_x\rangle \langle \phi_x|$  is the density matrix corresponding to the ensemble  $\mathcal{E}$  and  $\Upsilon_{(a,p)}$  is a Hermitian operator defined as [TEDMF13]:

$$\Upsilon_{(a,p)} := -i \frac{\partial U^\dagger(\boldsymbol{\theta})}{\partial \boldsymbol{\theta}_{(a,p)}} U(\boldsymbol{\theta}) = i U^\dagger(\boldsymbol{\theta}) \frac{\partial U(\boldsymbol{\theta})}{\partial \boldsymbol{\theta}_{(a,p)}}.$$

A detailed proof is provided in Appendix C. It can be easily seen that the  $\mathcal{F}^{\mathcal{E}}$  metric reduces to the Fubini-Study metric for pure quantum states, i.e., if the input ensemble  $\mathcal{E} = \{(1, |\phi\rangle)\}$  then  $\mathcal{F}^{\mathcal{E}} = \mathsf{F}^\phi$ . In this sense, E-QFIM can be considered as a generalization of the Fubini-Study metric to an ensemble of quantum states.

For the PQC model described in Section II, we can derive an explicit expression for  $\mathcal{F}^{\mathcal{E}}$ , where each of its elements can be expressed as the covariance of certain observables with respect to the density matrix  $\rho$  as given by the following lemma.

**Lemma 1.** *For a parameterized unitary operator  $U(\theta)$  discussed in Section II and an ensemble  $\{(Q_X(x), |\phi_x\rangle)\}$  with the corresponding the density matrix  $\rho$ , the entry of E-QFIM is obtained as*

$$\mathcal{F}_{(a_p, b_q)}^{\mathcal{E}}(\theta) = \text{Cov}(G_{a_p}, G_{b_q})_{\rho} \quad (16)$$

where  $G_{a_p} := W_{[1:a]}^\dagger(\mathbb{I}^{\otimes[1:p]} \otimes (\sigma_p^a/2) \otimes \mathbb{I}^{\otimes(p:d)})W_{(a:1)}$  is a Hermitian matrix<sup>4</sup>,  $G_{a_p}^2 = G_{b_q}^2 = \mathbb{I}/4$ , and  $\text{Cov}(G_{a_p}, G_{b_q})_{\rho}$  denotes the covariance between  $G_{a_p}$  and  $G_{b_q}$  on density matrix  $\rho$  given as:

$$\text{Cov}(G_{a_p}, G_{b_q})_{\rho} := \frac{1}{2} \text{Tr}(\{G_{a_p}, G_{b_q}\}\rho) - \text{Tr}(G_{a_p}\rho) \text{Tr}(G_{b_q}\rho). \quad (17)$$

*Proof.* The complete derivation is provided in Appendix D.  $\square$

### B. Quantum Natural Stochastic Pairwise Coordinate Descent

In this subsection, we introduce the novel and physically realizable variant of QNGD, namely, the Quantum Natural Stochastic Pairwise Coordinate Descent (2-QNSCD) algorithm. 2-QNSCD is an information geometry-based optimization method with the following update rule:

$$\theta^{(t+1)} = \theta^{(t)} - \eta_t \bar{\mathbf{Z}}^t(a_p, b_q)^{-1} \mathbf{g}^t(a_p, b_q). \quad (18)$$

Here,  $a_p$  and  $b_q$  are distinct coordinates randomly chosen from the set  $[c]$ ,  $\eta_t$  denotes the learning rate,  $\bar{\mathbf{Z}}^t(a_p, b_q)$  is a random  $c \times c$  matrix resulting from an E-QFIM measurement with the following sparse structure. All the off-diagonal entries of the matrix  $\bar{\mathbf{Z}}^t$  are zero except the entries corresponding to coordinates  $(a_p, b_q)$  and  $(b_q, a_p)$ . Additionally,  $\mathbf{g}^t(a_p, b_q)$  is a random  $c \times 1$  vector obtained from a gradient measurement. It contains only two non-zero entries corresponding to coordinates  $a_p$  and  $b_q$ . In this approach, there are three levels of stochasticity: (a) the selection of the input quantum state, (b) the selection of the coordinate pair, and (c) the measurement outcome of a quantum circuit.

2-QNSCD selects two coordinates, denoted as  $a_p$  and  $b_q$ , and constructs a random vector  $\mathbf{g}^{(t)}(a_p, b_q)$  of length  $c$  using a quantum circuit. This vector serves as an estimator of the gradient of  $\mathcal{L}(\theta^{(t)})$ . Moreover,

<sup>4</sup>For brevity, throughout the paper, we refrain from explicitly showing the dependence on parameters  $\theta$ . Nonetheless, it should be clear from the context.

it is required to be an unbiased estimator, i.e.,  $\mathbb{E}[\mathbf{g}^{(t)}(\mathbf{a}_p, \mathbf{b}_q)] = \nabla \mathcal{L}(\boldsymbol{\theta}^{(t)})$ , where the expectation is taken over the choice of the coordinate pair  $(\mathbf{a}_p, \mathbf{b}_q)$ , the measurement outcome of a gradient estimation circuit, and the input quantum states. Then, it constructs a positive definite matrix  $\bar{\mathbf{Z}}^t(\mathbf{a}_p, \mathbf{b}_q)$  of size  $c \times c$  using another quantum circuit, and it is required to be an unbiased estimator of  $\mathcal{F}^{\mathcal{E}}$ , i.e.,  $\mathbb{E}[\bar{\mathbf{Z}}^t(\mathbf{a}_p, \mathbf{b}_q)] = \mathcal{F}^{\mathcal{E}}(\boldsymbol{\theta}^{(t)})$ . Here, the expectation is over the choice of the pair of coordinates  $(\mathbf{a}_p, \mathbf{b}_q)$ , the measurement outcome of an E-QFIM estimation circuit, and the input quantum states. Finally, we emphasize that in the update rule (18) only two coordinates of PQC parameters  $\boldsymbol{\theta}$ , particularly,  $\boldsymbol{\theta}_{(a,p)}$  and  $\boldsymbol{\theta}_{(b,q)}$  are updated. The quantum circuits for generating  $\bar{\mathbf{Z}}(\mathbf{a}_p, \mathbf{b}_q)$  and  $\mathbf{g}(\mathbf{a}_p, \mathbf{b}_q)$  are discussed in the following subsections.

In the next two subsections, we present a series of quantum circuits to estimate  $\mathcal{F}^{\mathcal{E}}$  and  $\nabla \mathcal{L}$  independently and separately. Our estimation has a constant overhead, as it only uses 6 samples per iteration of the 2-QNSCD algorithm: four for the metric and two for the gradient. This is a significant reduction compared to conventional estimation processes using repeated measurements to approximate the expectation involved in computing the gradient of the loss function and the quantum information metric tensor.

1) **Estimation of the Metric:** Randomly select a pair of coordinates  $(\mathbf{a}_p, \mathbf{b}_q)$  corresponding to the parameters  $\boldsymbol{\theta}_{(a,p)}$  and  $\boldsymbol{\theta}_{(b,q)}$ , respectively. Then, consider a  $2 \times 2$  sub-matrix of  $\mathcal{F}^{\mathcal{E}}$  corresponding to the parameters  $\boldsymbol{\theta}_{(a,p)}$  and  $\boldsymbol{\theta}_{(b,q)}$ , which we denote as  $\mathcal{F}_{[\mathbf{a}_p, \mathbf{b}_q]}^{\mathcal{E}}$ . Thus, from (16) it follows:

$$\mathcal{F}_{[\mathbf{a}_p, \mathbf{b}_q]}^{\mathcal{E}} = \begin{bmatrix} 0.25 - [\text{Tr}(G_{\mathbf{a}_p} \rho)]^2 & \text{Cov}(G_{\mathbf{a}_p}, G_{\mathbf{b}_q})_{\rho} \\ \text{Cov}(G_{\mathbf{a}_p}, G_{\mathbf{b}_q})_{\rho} & 0.25 - [\text{Tr}(G_{\mathbf{b}_q} \rho)]^2 \end{bmatrix}. \quad (19)$$

We first construct a  $c \times c$  random matrix  $\mathbf{Z}(\mathbf{a}_p, \mathbf{b}_q)$  such that its submatrix  $\mathbf{Z}_{[\mathbf{a}_p, \mathbf{b}_q]}$  is an unbiased estimate of  $\mathcal{F}_{[\mathbf{a}_p, \mathbf{b}_q]}^{\mathcal{E}}$ , and all other entries of  $\mathbf{Z}$  are zero. Subsequently, through some post-processing steps, we derive an unbiased estimate of  $\mathcal{F}^{\mathcal{E}}$ , denoted as  $\bar{\mathbf{Z}}(\mathbf{a}_p, \mathbf{b}_q)$ <sup>5</sup>. Now, the construction of  $\mathbf{Z}_{[\mathbf{a}_p, \mathbf{b}_q]}$  involves designing estimators for  $\text{Tr}(G_{\mathbf{a}_p} \rho)$ ,  $\text{Tr}(G_{\mathbf{b}_q} \rho)$ ,  $[\text{Tr}(G_{\mathbf{a}_p} \rho)]^2$ ,  $[\text{Tr}(G_{\mathbf{b}_q} \rho)]^2$ , and  $\text{Tr}(\{G_{\mathbf{a}_p}, G_{\mathbf{b}_q}\} \rho)$ . To understand this process, without loss of generality, we assume  $a \leq b$ . Let  $z_{11}, z_{12}, z_{21}, z_{22}$  be the elements of the matrix  $\mathbf{Z}_{[\mathbf{a}_p, \mathbf{b}_q]}$ . In the following, we use four samples  $\{|\phi_{x_i}\rangle\}_{i \in [4]}$  to construct these elements. We provide a method to estimate the entries of the matrix as follows:

**Estimator  $z_{22}$ :** We independently apply the first  $(b-1)$  layers of the PQC on the first two samples  $|\phi_{x_1}\rangle$  and  $|\phi_{x_2}\rangle$ . Then, measure the  $q^{\text{th}}$  qubit along the basis of  $\sigma_q^b$ . Let  $(v_1, v_2) \in \{-1, +1\}^2$  be the outcomes corresponding to the first and second measurements, respectively. Then, we compute  $z_{22} := 0.25 \cdot (1 - v_1 v_2)$ .

This amounts to creating an estimator for a term of the form  $(\mathbb{E}[A])^2$ , where  $A$  is a random variable with a probability distribution  $P_A$ . To accomplish this, generate a pair of independent random variables  $A_1$  and  $A_2$

<sup>5</sup>For ease of notation, we drop the dependence of estimators  $\mathbf{Z}$  and  $\bar{\mathbf{Z}}$  on the pair of coordinates  $(\mathbf{a}_p, \mathbf{b}_q)$  when it is clear from the context.

with the distribution  $P_A$ . By taking the product  $A_1 A_2$ , we obtain an unbiased estimator for  $(\mathbb{E}[A])^2$ . In this context, the measurement outcomes are treated as these independent random variables, and their product is used to form the desired estimator.

For the off-diagonal terms,  $z_{12} = z_{21}$  (due to the symmetry of  $\mathcal{F}^{\mathcal{E}}$ ), it is not straightforward to measure the Cov term in the off-diagonal entries of  $\mathcal{F}_{[a_p, b_q]}^{\mathcal{E}}$  because Cov contains the anti-commutator term. Nonetheless, we address this issue by providing a sequential measurement strategy to estimate the expectation of the anti-commutator, given below. Moreover, using this sequential strategy, we can construct estimator  $z_{11}$  as a bonus.

**Lemma 2** (Sequential Measurement for Anti-Commutator). *Consider Hermitian matrices  $\mathbf{A}$  and  $\mathbf{B}$  on  $\mathcal{H}^d$ , such that  $\mathbf{A}^2 = \mathbb{I}$ , i.e.,  $\mathbf{A}$  has only two eigenvalues  $\pm 1$ , and the eigenvectors corresponding to these eigenvalues form a complete orthonormal basis for  $\mathcal{H}^d$ . Given a quantum state  $|\phi\rangle \in \mathcal{H}^d$ , the expectation of anti-commutator  $\{\mathbf{A}, \mathbf{B}\}$ , i.e.,  $\langle \phi | \{\mathbf{A}, \mathbf{B}\} | \phi \rangle$ , can be computed using the following sequential measurement strategy:*

- I. Perform a measurement on the state  $|\phi\rangle$  along the eigenvectors of  $\mathbf{A}$ , given as  $\mathcal{M} := \{\mathbf{A}_+, \mathbf{A}_-\}$ , where  $\mathbf{A}_+$  and  $\mathbf{A}_-$  are projectors onto eigenspace of  $\mathbf{A}$  corresponding to  $+1$  and  $-1$  eigenvalues, respectively.
- II. Measure the collapsed (post-measurement) state along the eigenvectors of  $\mathbf{B}$ .

Suppose  $A$  and  $B$  are random variables denoting the measurement outcomes of Steps I and II, respectively. Then the following equality holds:  $\frac{1}{2} \langle \phi | \{\mathbf{A}, \mathbf{B}\} | \phi \rangle = \mathbb{E}[AB]$ .

*Proof.* The proof is provided in Appendix E. □

**Estimators**  $z_{12}, z_{11}$ : Using the above sequential strategy, for each of the remaining samples  $|\phi_{x_3}\rangle$  and  $|\phi_{x_4}\rangle$ , we independently apply the first  $(a-1)$  layers of the PQC and measure the  $p^{\text{th}}$  qubit along the eigenvectors of  $\sigma_p^a$ . The collapsed (post-measured) state is then passed through layer  $a$  up to layer  $(b-1)$  of the PQC, and the  $q^{\text{th}}$  qubit of the output state is measured along the eigenvectors of  $\sigma_q^b$ . Let  $(u_1, w_1), (u_2, w_2) \in \{-1, +1\}$  be the first and second measurement outcomes for  $|\phi_{x_3}\rangle$  and  $|\phi_{x_4}\rangle$ , respectively. Then, we compute off-diagonal entries as follows:  $z_{21} = z_{12} := 0.125 \cdot (u_1 w_1 + u_2 w_2) - 0.0625 \cdot (u_1 + u_2)(v_1 + v_2)$ . Finally, we compute the diagonal term  $z_{11} := 0.25 \cdot (1 - u_1 u_2)$ .

Now, combining these estimators, we obtain the matrix  $\mathbf{Z}_{[a_p, b_q]}$ . The following lemma shows that  $\mathbf{Z}_{[a_p, b_q]}$  yields an unbiased estimator of  $\mathcal{F}_{[a_p, b_q]}^{\mathcal{E}}$ .

**Lemma 3** (Unbiased Estimator of  $\mathcal{F}_{[a_p, b_q]}^{\mathcal{E}}$ ). *For a given pair of coordinates  $(a_p, b_q)$ , let  $\mathbf{Z}_{[a_p, b_q]}$  be the matrix generated from the above process. Then,  $\mathbb{E} [\mathbf{Z}_{[a_p, b_q]}] = \mathcal{F}_{[a_p, b_q]}^{\mathcal{E}}$ , where the expectation is over measurements outcomes and input quantum states.*

*Proof.* The proof is provided in Appendix F.  $\square$

**Estimator of  $\mathcal{F}^E$ :** After constructing the submatrix  $\mathbf{Z}_{[a_p, b_q]}$ , we now aim to construct a non-singular and unbiased estimator of the entire E-QFIM matrix. To achieve this, we introduce a positive parameter  $\beta > 0$ , which serves as a regularization constant.

Toward this, scale the diagonal terms of  $\mathbf{Z}_{[a_p, b_q]}$  by  $\frac{1}{(c-1)}$  and add  $\beta$  to it. This yields a  $2 \times 2$  matrix, denoted as  $\tilde{\mathbf{Z}}_{[a_p, b_q]}$ . The remaining  $c \times c$  matrix  $\tilde{\mathbf{Z}}$  is completed with zeros as other entries. Finally, we construct the estimator of  $\mathcal{F}^E$  as

$$\bar{\mathbf{Z}}(a_p, b_q) := \frac{c(c-1)}{2} \left( \tilde{\mathbf{Z}} - \frac{2\beta}{c} \mathbb{I} \right). \quad (20)$$

Here,  $\mathbb{I}$  denotes  $c \times c$  identity matrix. The parameter  $\beta$  is used to ensure the positive definiteness of  $\bar{\mathbf{Z}}_{[a_p, b_q]}$ , which primarily contributes to the update rule of 2-QNSCD. It prevents the condition number of the random matrix  $\bar{\mathbf{Z}}_{[a_p, b_q]}$  from scaling with the number of model parameters and thus mitigates any numerical instability. Moreover, it can be easily seen that the gate complexity for constructing the unbiased estimator of  $\mathcal{F}^E$  is, at most, the gate complexity of  $U(\theta)$ . This procedure is summarized in Algorithm 1. The following lemma shows that the final matrix  $\bar{\mathbf{Z}}(a_p, b_q)$  obtained after the classical post-processing of  $\mathbf{Z}_{[a_p, b_q]}$  is an unbiased estimator of  $\mathcal{F}^E$ .

**Theorem 2** (Unbiased Estimation of  $\mathcal{F}^E$ ). *Let  $\bar{\mathbf{Z}}(a_p, b_q)$  be the matrix generated from the above process for a pair of randomly selected coordinates  $(a_p, b_q)$ . The expectation of  $\bar{\mathbf{Z}}(a_p, b_q)$  over the choice of a pair of coordinates, measurements outcome, and input quantum states satisfies:*

$$\mathbb{E}[\bar{\mathbf{Z}}(a_p, b_q)] = \mathcal{F}^E.$$

*Proof.* The proof is provided in Appendix G.  $\square$

This completes the construction of an unbiased estimator of the E-QFIM. Next, we design an unbiased estimator of the gradient of the loss function.

2) **Estimation of the Gradient:** We begin by computing the derivative of the per-sample expected loss with respect to  $\theta_{(a,p)}$ , which can be expressed as

$$\partial_{a_p} \mathcal{L}(\theta, |\phi_x\rangle, y) = \sum_{\hat{y} \in \mathcal{Y}} -\frac{i}{2} \ell(y, \hat{y}) \text{Tr}\{\Lambda_{\hat{y}} W_{[L:a]} [\Sigma_p^a, \Phi_x^a] W_{[a:L]}^\dagger\},$$

where  $\Phi_x^a := W_{(a:1]} \Phi_x W_{[1:a]}^\dagger$  and  $\Sigma_p^a := (\mathbb{I}^{\otimes[1:p]} \otimes \sigma_p^a \otimes \mathbb{I}^{\otimes(p:d)})$ . We provide the derivation in Appendix H. Here, note that the derivative involves a commutator term, which poses a challenge because it is an anti-Hermitian matrix and cannot be measured directly. Addressing this challenge, the authors in [HGS22]

---

**Algorithm 1:** One-Shot E-QFIM Estimator
 

---

```

1 Function E-QFIM_Estimator ( $\{|\phi_{x_i}\rangle\}_{i \in [4]}$ ,  $a_p, b_q, \beta$ ):
  2   %%  $\{|\phi_{x_i}\rangle\}_{i \in [4]}$  : i.i.d. quantum samples
  3   %%  $(a_p, b_q)$  : a random pair of distinct coordinates (assume  $a \leq b$ )
  4   %%  $\beta > 0$  : regularization constant
  5   /* Consider  $|\phi_{x_1}\rangle$  and  $|\phi_{x_2}\rangle$  */
```

**for**  $i = 1$  to  $2$  **do**
**6** Apply the first  $(b-1)$  layers of  $U(\theta)$  on  $|\phi_{x_i}\rangle$ 
**7** Measure  $q^{\text{th}}$  qubit along the eigenvectors of  $\sigma_q^b$ 
**8**  $v_i \in \{-1, +1\} \leftarrow$  measurement outcome
**9** /\* Consider  $|\phi_{x_3}\rangle$  and  $|\phi_{x_4}\rangle$  \*/
**for**  $i = 3$  to  $4$  **do**
**10** Apply the first  $(a-1)$  layers of  $U(\theta)$  on  $|\phi_{x_i}\rangle$ 
**11** Measure  $p^{\text{th}}$  qubit along the eigenvectors of  $\sigma_p^a$ 
**12**  $u_i \in \{-1, +1\} \leftarrow$  measurement outcome
 **13**  $|\phi_{x_i}^a\rangle \leftarrow$  post-measured state
 **14** Apply layers from  $a$  to  $(b-1)$  of  $U(\theta)$  on  $|\phi_{x_i}^a\rangle$ 
**15** Measure  $q^{\text{th}}$  qubit along the eigenvectors of  $\sigma_q^b$ 
**16**  $w_i \in \{-1, +1\} \leftarrow$  measurement outcome
 /\* Construct E-QFIM estimator \*/
**17**  $\tilde{\mathbf{Z}} \leftarrow 0_{c \times c}$  (all-zero matrix)
**18**  $\tilde{\mathbf{Z}}_{[a_p, b_q]} = \begin{bmatrix} \frac{(1-u_1 u_2)}{4 \cdot (c-1)} + \beta & \frac{(u_1 w_1 + u_2 w_2)}{8} - \frac{1}{4} \frac{(u_1 + u_2)}{2} \frac{(v_1 + v_2)}{2} \\ \frac{(u_1 w_1 + u_2 w_2)}{8} - \frac{1}{4} \frac{(u_1 + u_2)}{2} \frac{(v_1 + v_2)}{2} & \frac{(1-v_1 v_2)}{4 \cdot (c-1)} + \beta \end{bmatrix}$ 
**19** **return**  $\mathbf{Z} := \frac{c(c-1)}{2} (\tilde{\mathbf{Z}} - (\frac{2\beta}{c}) \mathbb{I})$ 


---

introduced an innovative approach to constructing an unbiased estimate for the commutator, hence for the gradient. Below, we present a lemma summarizing the gradient estimation method proposed in [HGS22].

**Lemma 4** (Observable for Commutator). *Consider Hermitian matrices  $\mathbf{A}$  and  $\mathbf{B}$  on  $\mathcal{H}^d$ , such that  $\mathbf{A}^2 = \mathbb{I}$ , i.e.,  $\mathbf{A}$  has only two eigenvalues  $\pm 1$ , and the eigenvectors corresponding to these eigenvalues form a complete orthonormal basis for  $\mathcal{H}^d$ . For a given quantum state  $|\phi\rangle \in \mathcal{H}^d$ , the expectation of commutator  $[\mathbf{A}, \mathbf{B}]$  can be expressed as  $\langle \phi | [\mathbf{A}, \mathbf{B}] | \phi \rangle = 2i \langle \tilde{\phi} | \mathbf{V}^\dagger O \mathbf{V} | \tilde{\phi} \rangle$ , where  $|\tilde{\phi}\rangle := |\phi\rangle \otimes |+\rangle$ ,  $O$  is an observable, and  $\mathbf{V}$  is a unitary operator defined as:*

$$O := \mathbf{B} \otimes |0\rangle\langle 0| - \mathbf{B} \otimes |1\rangle\langle 1| \quad \text{and} \quad \mathbf{V} := e^{i\pi\mathbf{A}/4} \otimes |0\rangle\langle 0| + e^{-i\pi\mathbf{A}/4} \otimes |1\rangle\langle 1|.$$

*Proof.* The proof relies on [HGS22, Lemma 1]. For completeness, a detailed proof is given in Appendix I.  $\square$

We are now equipped to discuss the method for constructing an estimator of the gradient using only two samples. Consider a pair of coordinates  $(a_p, b_q)$  corresponding to the parameters  $\theta_{(a,p)}$  and  $\theta_{(b,q)}$ . We use two samples along with their true labels  $(|\phi_{x_1}\rangle, y_1)$  and  $(|\phi_{x_2}\rangle, y_2)$  to construct estimators  $g_{a_p}$  and  $g_{b_q}$  corresponding to these parameters, respectively. The method is as follows:

**Estimator  $g_{a_p}$ :** We apply the first  $(a-1)$  layers of the PQC and add an ancilla qubit  $|+\rangle$  to the output quantum state  $|\phi_{x_1}^a\rangle$ . This creates the state  $\tilde{\Phi}_{x_1}^a := (W_{(a:1]}\Phi_{x_1}W_{[1:a]}^\dagger) \otimes |+\rangle\langle+|$ . Then, we apply the following unitary matrix  $\mathbf{V} := e^{i\pi\Sigma_p^a/4} \otimes |0\rangle\langle 0| + e^{-i\pi\Sigma_p^a/4} \otimes |1\rangle\langle 1|$  on  $\tilde{\Phi}_{x_1}^a$ . Next, we apply the remaining layers of the PQC on the state  $\mathbf{V}\tilde{\Phi}_{x_1}^a\mathbf{V}^\dagger$ , and measure the state by the quantum measurement  $\tilde{\Lambda} := \{\Lambda_{\hat{y}} \otimes |b\rangle\langle b| : \hat{y} \in \mathcal{Y}, b \in \{0, 1\}\}$ . Let  $(\hat{y}, b)$  be the outcome of the measurement. Finally, we compute  $g_{a_p} := (-1)^{(1+b)}\ell(y_1, \hat{y})$ .

**Estimator  $g_{b_q}$ :** Following a similar procedure as for  $g_{a_p}$ , we construct  $g_{b_q}$  with the correspondence  $a_p \leftrightarrow b_q$  and using the pair  $(|\phi_{x_2}\rangle, y_2)$ . Note that, using Lemma 4, one can easily show

$$\mathbb{E}[g_{a_p} || |\phi_{x_1}\rangle, y_1] = \nabla \mathcal{L}_{(a,p)}(\theta, |\phi_{x_1}\rangle, y_1) \text{ and } \mathbb{E}[g_{b_q} || |\phi_{x_2}\rangle, y_2] = \nabla \mathcal{L}_{(b,q)}(\theta, |\phi_{x_2}\rangle, y_2), \quad (21)$$

where the expectation is over the measurement outcome and the input quantum state.

**Estimator of  $\nabla \mathcal{L}$ :** After constructing  $g_{a_p}$  and  $g_{b_q}$ , we construct the estimator of  $\nabla \mathcal{L}$  as

$$\mathbf{g}(a_p, b_q) := \left(\frac{c}{2}\right) (g_{a_p} \mathbf{e}_{a_p} + g_{b_q} \mathbf{e}_{b_q}), \quad (22)$$

where  $\mathbf{e}_{a_p}$  and  $\mathbf{e}_{b_q}$  represent unit vectors corresponding to  $a_p$  and  $b_q$ , respectively. This gradient estimation procedure is summarized in Algorithm 2. The following lemma demonstrates that  $\mathbf{g}(a_p, b_q)$  provides an unbiased estimate of  $\nabla \mathcal{L}$ .

**Proposition 1** (Unbiased Estimation of  $\nabla \mathcal{L}$ ). *Let  $\mathbf{g}(a_p, b_q)$  be the vector generated from the above process for a pair of randomly selected coordinates  $(a_p, b_q)$ . The expectation of  $\mathbf{g}(a_p, b_q)$  over the choice of the pair of coordinates, measurements outcome, and input quantum states satisfies:*

$$\mathbb{E}[\mathbf{g}(a_p, b_q)] = \nabla \mathcal{L}.$$

*Proof.* The proof is provided in Appendix J. □

3) **2-QNSCD Update Rule:** We construct the following algorithm that updates only two randomly selected parameters (indexed by  $a_p$  and  $b_q$ ) at each iteration. For that, we use 6 samples to perform one iteration of the update presented as follows:

$$\theta^{(t+1)} = \theta^{(t)} - \eta_t |\bar{\mathbf{Z}}^t(a_p, b_q)|^{-1} \mathbf{g}^t(a_p, b_q), \quad (23)$$

---

**Algorithm 2:** One-Shot Gradient Estimator

---

```

1 Function Gradient_Estimator ( $\{(|\phi_{x_i}\rangle, y_i)\}_{i \in [2]}, a_p, b_q$ ) :
2   %%  $\{(|\phi_{x_i}\rangle, y_i)\}_{i \in [2]}$  : i.i.d. quantum samples with true labels
3   %%  $(a_p, b_q)$  : a random pair of distinct coordinates (assume  $a \leq b$ )
4   Let  $l_1 \leftarrow a$  and  $l_2 \leftarrow b$ 
      /* Consider  $|\phi_{x_1}\rangle$  and  $|\phi_{x_2}\rangle$ 
5   for  $i = 1$  to  $2$  do
6     Apply the first  $(l_i - 1)$  layers of  $U(\theta)$  on  $|\phi_{x_i}\rangle$ 
7     Add an ancilla qubit  $|+\rangle$  to output of layer  $(l_i - 1)$ 
8      $(\Phi_{x_i}^{l_i} \otimes |+\rangle\langle+|) \leftarrow$  output state
9     Apply  $V := e^{i\pi\Sigma_p^a/4} \otimes |0\rangle\langle 0| + e^{-i\pi\Sigma_p^a/4} \otimes |1\rangle\langle 1|$  on  $(\Phi_{x_i}^{l_i} \otimes |+\rangle\langle+|)$ 
10    Apply layers from  $l_i$  to  $L$  on  $V(\Phi_{x_i}^{l_i} \otimes |+\rangle\langle+|)V^\dagger$ 
11    Measure the resulting state with  $\{\Lambda_{\hat{y}} \otimes |b\rangle\langle b| : \hat{y} \in \mathcal{Y}, b \in \{0, 1\}\}$ 
12     $(\hat{y}_i, b_i) \leftarrow$  measurement outcomes
13     $g_{a_p} \leftarrow (-1)^{(1+b_1)} \ell(\hat{y}_1, y_1)$ 
14     $g_{b_q} \leftarrow (-1)^{(1+b_2)} \ell(\hat{y}_2, y_2)$ 
15   return  $g(a_p, b_q) := \left(\frac{c}{2}\right) (g_{a_p} e_{a_p} + g_{b_q} e_{b_q})$ 

```

---

where  $\eta_t$  is the learning rate,  $|\bar{Z}| := \sqrt{\bar{Z}^\dagger \bar{Z}}$ , and  $\beta$  is chosen according to Remark 1 as stated below. Because of the structure of  $\bar{Z}$  and  $g$ , (23) can be re-written as

$$[\theta_{(a,p)}^{(t+1)}, \theta_{(b,q)}^{(t+1)}]^\top \leftarrow [\theta_{(a,p)}^{(t)}, \theta_{(b,q)}^{(t)}]^\top - \eta_t \left| \tilde{Z}_{[a_p, b_q]}^t - \left(\frac{2\beta}{c}\right) \mathbb{I}_2 \right|^{-1} [g_{a_p}^t, g_{b_q}^t]^\top, \quad (24)$$

where  $\mathbb{I}_2$  is the  $2 \times 2$  identity matrix and  $\eta_t$  contains the normalizing constant  $(c-1)$ .

**Remark 1.** It is important to note that, given the structure of  $\bar{Z}$ , by appropriately choosing  $\beta$ , the sub-matrix  $(\tilde{Z}_{[a_p, b_q]} - (\frac{2\beta}{c}) \mathbb{I}_2)$  can be made positive definite (PD) with probability 1.

Moreover, from the description of the 2-QNSCD algorithm in (24), it is evident that only  $(\tilde{Z}_{[a_p, b_q]} - (\frac{2\beta}{c}) \mathbb{I}_2)$  contributes to the update of parameters. Therefore, for a given  $c$ , choosing an appropriate  $\beta$ , using Remark 1, makes the use of  $|\bar{Z}^t|$  equivalent to that of  $\bar{Z}^t$  in the update rule (23). However, we keep the former for the sake of mathematical rigor. The 2-QNSCD algorithm is summarized in Algorithm 3.

### C. Convergence Analysis of 2-QNSCD

We now present the convergence analysis of the 2-QNSCD algorithm. In particular, we demonstrate that 2-QNSCD exhibits exponential convergence to the optimal parameter values given that the underlying objective

**Algorithm 3:** 2-QNSCD

---

**Input:** Training data  $\{(|\phi_t\rangle, y_t)\}_{t=0}^{(6n-1)}$ , learning rate  $\eta_t$ , and regularization constant  $\beta > 0$

**Output:** Updated PQC parameters:  $\theta^{(n)}$

```

/* Initialization
1 Randomly select the parameters  $\theta^{(0)}$  over  $[0, 2\pi]^c$ 
2 for  $t = 0$  to  $(n - 1)$  do
3   Randomly select a pair of coordinates  $(a_p, b_q)$ 
4    $\mathbf{g}^t(a_p, b_q) = \text{Gradient\_Estimator}(\{(|\phi_{(6t+k)}\rangle, y_{(6t+k)})\}_{k \in \{0,1\}})$ 
5    $\bar{\mathbf{Z}}^t(a_p, b_q) = \text{E-QFIM\_Estimator}(\{|\phi_{(6t+k)}\rangle\}_{k \in [2:5]}, a_p, b_q)$ 
6   Update the parameter as :
7    $\theta^{(t+1)} \leftarrow \theta^{(t)} - \eta_t |\bar{\mathbf{Z}}^t(a_p, b_q)|^{-1} \mathbf{g}^t(a_p, b_q)$ 
8 return  $\theta$ 

```

---

function is bounded, pairwise  $L_2$ -smooth, and satisfies a modified version of PL inequality (see Definition 3). Before presenting the convergence theorem, we state the following assumptions on the loss function  $\mathcal{L}(\theta)$ .

**Assumption 1.** (Pairwise  $L_2$ -smooth) The function  $\mathcal{L}(\theta)$  is pairwise  $L_2$ -smooth (or has a pairwise  $L_2$ -Lipchitz continuous gradient), i.e., for all pair of coordinates  $(i, j) \in [c]^2$ ,  $\theta \in \mathbb{R}^c$ , and  $\alpha_i, \alpha_j \in \mathbb{R}$ , we have

$$\mathcal{L}(\theta + (\alpha_i \mathbf{e}_i + \alpha_j \mathbf{e}_j)) \leq \mathcal{L}(\theta) + \nabla \mathcal{L}(\theta)^\top (\alpha_i \mathbf{e}_i + \alpha_j \mathbf{e}_j) + \frac{L_2}{2} \|\alpha_i \mathbf{e}_i + \alpha_j \mathbf{e}_j\|^2.$$

**Assumption 2.** Let  $\theta^* \in \mathbb{R}^c$  be the global minimum of the loss function  $\mathcal{L}$ . For all  $\theta \in \mathbb{R}^c$ , it holds that

$$\frac{1}{2} \nabla \mathcal{L}(\theta)^\top \left( \frac{2}{c(c-1)} \mathcal{F}^{\mathcal{E}}(\theta) + \frac{4(c-2)}{c^2} \beta \mathbb{I} \right)^{-1} \nabla \mathcal{L}(\theta) \geq \bar{\mu} (\mathcal{L}(\theta) - \mathcal{L}(\theta^*)), \quad \text{for some } \bar{\mu} > 0.$$

The second assumption can be considered as a regularized version of QGI inequality (see Definition 4)<sup>6</sup>. Below, we state the 2-QNSCD convergence theorem, where we refer to these assumptions in the proof.

**Theorem 3** (Convergence of 2-QNSCD). *Under the assumption mentioned above, 2-QNSCD with a fixed learning rate  $\eta = \beta/L_2$ , number of parameters  $c > 2$ , and the update rule (23) achieves a global exponential convergence rate, given by,*

$$\mathbb{E}[\mathcal{L}(\theta^{(t)}) - \mathcal{L}(\theta^*)] \leq \left(1 - \frac{8\bar{\mu}\beta}{c^3 L_2}\right)^t (\mathcal{L}(\theta^{(0)}) - \mathcal{L}(\theta^*)) + \frac{c}{8\bar{\mu}} \alpha^2 \beta^2, \quad (25)$$

where  $\alpha^2 = \max_{(i,j)} \mathbb{E}[\|\tilde{\mathbf{Z}}_{[i,j]}^t - (2\beta/c)\mathbb{I}_2\|^{-1}\|^2] \mathbb{E}[\|[g_i^t, g_j^t]\|^2]$ .

<sup>6</sup>The QGI inequality condition is independent of convexity, and it can be satisfied by non-convex functions with multiple saddle points. The QGI inequality is a slightly more general condition than the PL inequality. In Section VI, we present examples involving non-convex functions that satisfy the QGI inequality and do not satisfy the PL inequality.

*Proof.* The proof is provided in Appendix K.  $\square$

The theorem mentioned above demonstrates that 2-QNSCD achieves an exponential convergence rate without needing multiple identical copies of a quantum state, repeated measurements, and  $O(c^2)$  cost of computing a metric tensor. The proof mainly relies on the structure of estimators  $\bar{\mathbf{Z}}$  and  $\mathbf{g}$  and uses inequalities such as the Kiefer inequality [Kie59].

## V. NUMERICAL RESULTS

In this section, we numerically assess the performance of the 2-QNSCD optimization method to train our QML model. In our experiments, we focus on the binary classification of quantum states with labels  $\{+1, -1\}$  and conventional 0-1 loss to measure the predictor's accuracy.

**Dataset Generation:** We use a synthetic dataset that generalizes the well-known dataset used in [MSB04] to multi-qubit systems. In the dataset generation process, first, consider the following three  $d$ -qubit quantum states:

$$|\phi_1(\mathbf{u})\rangle := \sum_{j=0}^{(2^d-2)/2} \frac{\mathbf{u}[j]}{\|\mathbf{u}\|} |\text{bin}(2j)\rangle, \quad |\phi_2(\mathbf{u})\rangle := \sum_{j=0}^{(2^d-2)/2} (-1)^{(j \bmod 2+1)} \frac{\mathbf{u}[j]}{\|\mathbf{u}\|} |\text{bin}(2j + 1_{\{j \bmod 2=0\}})\rangle,$$

$$|\phi_3(\mathbf{u})\rangle := \sum_{j=0}^{(2^d-2)/2} \frac{\mathbf{u}[j]}{\|\mathbf{u}\|} |\text{bin}(2j + 1_{\{j \bmod 2=0\}})\rangle,$$

where the vector  $\mathbf{u} \in [0, 1]^{2^{d-1}}$  and  $\text{bin}$  is the function that converts a decimal number to its binary representation. To understand the structure of the above quantum states, consider the case where  $d = 3$ . In this scenario, the quantum states are given as follows:

$$|\phi_1(\mathbf{u})\rangle = (\mathbf{u}[0] |000\rangle + \mathbf{u}[1] |010\rangle + \mathbf{u}[2] |100\rangle + \mathbf{u}[3] |110\rangle)/\|\mathbf{u}\|,$$

$$|\phi_2(\mathbf{u})\rangle = (-\mathbf{u}[0] |001\rangle + \mathbf{u}[1] |010\rangle - \mathbf{u}[2] |101\rangle + \mathbf{u}[3] |110\rangle)/\|\mathbf{u}\|,$$

$$|\phi_3(\mathbf{u})\rangle = (\mathbf{u}[0] |001\rangle + \mathbf{u}[1] |010\rangle + \mathbf{u}[2] |101\rangle + \mathbf{u}[3] |110\rangle)/\|\mathbf{u}\|.$$

The quantum states to be classified are:  $|\phi_1(\mathbf{u})\rangle$  with label  $y = +1$  and  $\{|\phi_2(\mathbf{u})\rangle, |\phi_3(\mathbf{u})\rangle\}$  with label  $y = -1$ . For each quantum sample, a state is generated from the set  $\{|\phi_1(\mathbf{u})\rangle, |\phi_2(\mathbf{u})\rangle, |\phi_3(\mathbf{u})\rangle\}$  with equal probability. This implies,  $\mathbb{P}\{y = -1\} = 2 \cdot \mathbb{P}\{y = +1\} = 2/3$ . Additionally, for each sample, the vector  $\mathbf{u}$  is selected randomly, independently, and with the uniform distribution on  $[0, 1]^{2^{d-1}}$ . For better understanding, Fig. 3 illustrates the dataset for the 2-qubit case.

**PQC Setup:** We consider four cases involving 3, 4, 5, and 6 qubits. For the 3-qubit case, the PQC consists of three parameterized layers of  $R_Y$  gates, alternating with three non-parameterized entangling layers. In the 4-qubit case, the PQC includes two parameterized layers of  $(R_Z \times R_Y)$  gates, each followed by an entangling

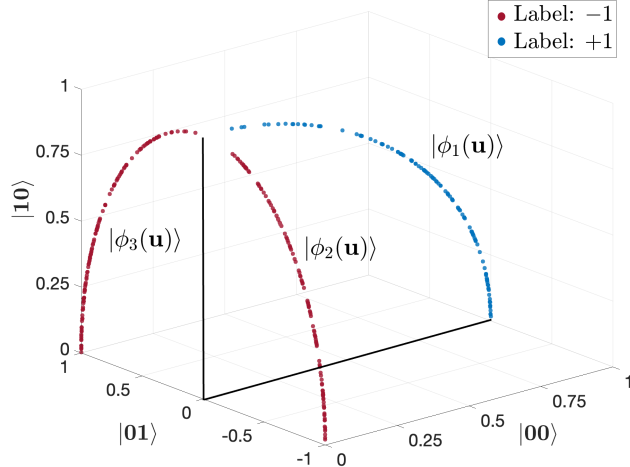


Figure 3: 2-qubit synthetic datasets, where the quantum states are given as  $|\phi_1(\mathbf{u})\rangle = (\mathbf{u}[0]|00\rangle + \mathbf{u}[1]|10\rangle)/\|\mathbf{u}\|$ ,  $|\phi_2(\mathbf{u})\rangle = (-\mathbf{u}[0]|01\rangle + \mathbf{u}[1]|10\rangle)/\|\mathbf{u}\|$ , and  $|\phi_3(\mathbf{u})\rangle = (\mathbf{u}[0]|01\rangle + \mathbf{u}[1]|10\rangle)/\|\mathbf{u}\|$ . The state  $|\phi_1(\mathbf{u})\rangle$  has label +1 and is colored in blue. The states  $|\phi_2(\mathbf{u})\rangle$  and  $|\phi_3(\mathbf{u})\rangle$  have label -1 and are colored in red.

layer. For the 5-qubit and 6-qubit cases, we explore two different circuits for each. The first PQC for both 5 and 6 qubits comprises three parameterized layers of  $(R_Z \times R_Y)$  gates, with an entangling layer after each parameterized layer. The second PQC for 5 qubits features six parameterized layers of alternating  $R_Y$  and  $R_Z$  gates, with an entangling layer after the first three parameterized layers. Similarly, the second PQC for 6 qubits consists of eight parameterized layers of alternating  $R_Y$  and  $R_Z$  gates, with an entangling layer placed after the first four parameterized layers. For convenience, the quantum circuit for 3 qubits is shown in Appendix L. The measurement used in the readout qubits has two outcomes  $\{+1, -1\}$ , each measured along the computational basis as  $\Lambda := \{\Lambda_{+1}, \Lambda_{-1} = (\mathbb{I} - \Lambda_{+1})\}$ , where

$$\Lambda_{+1} = |000\rangle\langle 000| + |011\rangle\langle 011| + |101\rangle\langle 101| + |110\rangle\langle 110|, \quad \text{for } d = 3, \text{ and}$$

$$\Lambda_{+1} = \sum_{j=0: (j \bmod 2=0)}^{2^d-1} |\text{bin}(j)\rangle\langle \text{bin}(j)|, \quad \text{for } d = 4, 5, 6.$$

For  $d = 3$ , this amounts to performing a complete measurement in the binary computational basis and then deciding  $\hat{y} = +1$  if the number of +1 observed is even. Otherwise, this amounts to performing a complete measurement in the decimal computational basis and then deciding  $\hat{y} = +1$  if the even outcome is observed.

**Experiment Results<sup>7</sup>:** To evaluate the 2-QNSCD performance, we utilize the PennyLane v0.34.0 open-source library [BIS<sup>+</sup>18] for implementing Algorithm 3. A constant learning rate of  $\eta = 2.5 \times 10^{-3}$  is used for all

<sup>7</sup>All the experimental results and source code implementations are available at <https://github.com/mdaamirQ/2-QNSCD>.

experiments. The initial parameters  $\theta^{(0)}$  are chosen randomly and independently from a uniform distribution over  $[0, 2\pi)^c$ . The regularization constant  $\beta$  is chosen as a sufficiently small positive number ensuring  $\bar{\mathbf{Z}}_{[i,j]}$  is positive definite for every pair of coordinates  $(i, j) \in [c]^2$ . For more detail, please refer to Appendix L.

*Demonstration of Training Progress:* To demonstrate the progress during the learning phase, we group samples into multiple batches of size  $N = 600$ . During each training step, we use a different batch, and the PQC processes every training sample of that batch and updates the model parameters accordingly. To investigate the speed of convergence, after each step, we compute the empirical loss of the PQC with the updated parameters given as

$$\mathcal{L}_{\text{Emp}}(\theta^{(i)}) = \frac{1}{N} \sum_{j=1}^N \mathbb{1}_{\{\hat{y}_j \neq y_j\}}(\theta^{(i)}), \quad (26)$$

where  $\hat{y}_j, y_j$  are the predicted and true labels, respectively, corresponding to the  $j^{\text{th}}$  sample of the batch, and  $\theta^{(i)}$  is the parameters at the end of  $i^{\text{th}}$  step. In addition, we compute the average of per-sample expected loss (as described in (7)) for all samples in the batch. We then plot the progress of training empirical loss and average per-sample expected loss against the number of steps.

*Comparison with different optimization schemes:* We compare the 2-QNSCD performance with the corresponding  $\Theta(1)$ -sample complexity variant of the gradient descent, namely, RQSGD (randomized quantum stochastic gradient descent) [HGS22]. With  $N = 600$ , the 2-QNSCD performs 100 parameter updates or iterations at each step. Therefore, to ensure a fair comparison, we provide 600 samples to RQSGD at each step to perform 100 iterations, but in two different ways. In the first method (2-RQSGD), six samples are used in each iteration to update only two parameters. Specifically, three samples are used to estimate the partial derivative of the loss function for each parameter. Let  $(a_p, b_q)$  be the pair of coordinates chosen at iteration  $t$ . Then, the estimate for  $\nabla \mathcal{L}_{a_p}(\theta^{(t)})$  is calculated as

$$g_{a_p}^t = \frac{1}{3} \sum_{j=1}^3 (-1)^{(1+b_j)} \ell(y_j, \hat{y}_j),$$

where  $y_j$ 's are true labels and  $(b_j, \hat{y}_j)$ 's are the measurement outcomes of the gradient estimation circuit (see Algorithm 2) corresponding to the three samples used. Similarly,  $g_{b_q}^t$  is calculated using the remaining three samples. Finally, the unbiased gradient estimator for 2-RQSGD is calculated as given in (22). In the second method (6-RQSGD), six samples are used in each iteration to update six parameters. Each sample is used to compute the estimate of the partial derivative of the loss function for one parameter, following a procedure similar to Algorithm 2 but applied to six coordinates. Let  $(j_1, j_2, \dots, j_6)$  be the six coordinates chosen at iteration  $t$ . Then, the unbiased estimator of the gradient for 6-RQSGD is calculated as  $\mathbf{g}^t = \left(\frac{c}{6}\right) (g_{j_1}^t \mathbf{e}_{j_1} + \dots + g_{j_6}^t \mathbf{e}_{j_6})$ .

Eventually, we compare the performance with the optimal expected loss within each batch. The closed-form

expression of the optimal expected loss is given as

$$\text{Optimal Expected Loss } \mathcal{L}_{\text{opt}} = \frac{1}{2} \left( 1 - \left\| \frac{1}{N} \sum_{j=1}^N y_j \Phi_{x_j} \right\|_1 \right), \quad (27)$$

where  $\{|\langle \phi_{x_j} \rangle|, y_j\}_{j=1}^N$  is the labeled quantum samples in a batch of size  $N$  and  $\|\cdot\|_1$  is the trace norm. The optimal expected loss for binary quantum state classification problem is derived in [HGS22, Lemma 3] using Holevo-Helstrom theorem [Hol12].

*Problem of exploding gradient and E-QFIM estimators:* While comparing the performance of 2-QNSCD with RQSGD, note that the gradient estimates grow with  $O(c)$  for a bounded loss function  $\ell(y, \hat{y})$ , whereas the elements of the inverse of the E-QFIM estimator diminishes with approximately  $O(c^2)$ . This implies, for RQSGD,  $\mathbf{g}$  explodes with  $O(c)$ , and for 2-QNSCD, the  $\bar{\mathbf{Z}}^{-1} \mathbf{g}$  roughly diminishes with  $O(c)$ . As a result, this discrepancy makes it challenging to directly compare RQSGD and 2-QNSCD. This issue of exploding and diminishing gradients has been observed in the training of classical neural networks, particularly in recurrent neural networks [BSF94]. Various methods have been proposed to address this problem, including gradient clipping, normalized parameter initialization, and re-scaling of the gradient [PMB13], [GB10], [GBC16]. Similarly, to circumvent the problem of diminishing and exploding estimates, we consider appropriately scaling the estimators with a global constant, ensuring that estimators neither explode nor diminish as  $c$  increases. This approach preserves the underlying structure of the estimators while preventing them from becoming unstable.

Figure 4 illustrates the performance comparison between 2-QNSCD, 2-RQSGD, and 6-RQSGD. Notably, 2-QNSCD converges nearly to the optimal loss faster than 2-RQSGD and 6-RQSGD. For 3Q (3-Qubit) and 4Q (4-Qubit) cases, Exp-1 and Exp-2 correspond to two different initial points. In 3Q Exp-1, 2-RQSGD probably gets trapped inside a local minimum or around a saddle point, whereas 6-RQSGD converges to the optimal loss. However, for nearly 100 steps, 6-RQSGD is stuck in a region where the gradient components are almost zero, whereas 2-QNSCD easily converges to optimal loss in just 70 steps. In 3Q Exp-2, both RQSGD and 2-QNSCD converge to the optimal loss, but 6-RQSGD and 2-RQSGD require roughly  $100 \times 600 = 6 \times 10^4$  and  $14 \times 10^4$  more samples than 2-QNSCD, respectively, to converge to the optimal loss.

In 4Q Exp-1, 2-RQSGD and 6-RQSGD are affected by the almost-zero gradient components region for nearly 140 steps. After this, 6-RQSGD drastically converges to the optimal loss, using roughly  $9 \times 10^4$  additional samples compared to 2-QNSCD, whereas 2-RQSGD fails to cross 60% accuracy even after using  $2.1 \times 10^5$  samples (i.e., 350 steps). In 4Q Exp-2, 2-RQSGD and 2-QNSCD get trapped in a region with almost-zero gradient components for nearly 100 steps. Afterward, 2-QNSCD quickly converges to the optimal loss, whereas 2-RQSGD barely crosses 60% accuracy after 350 steps. Although 6-RQSGD initially converges faster than 2-QNSCD and 2-RQSGD, it likely gets trapped around saddle points, local minima, or in a region

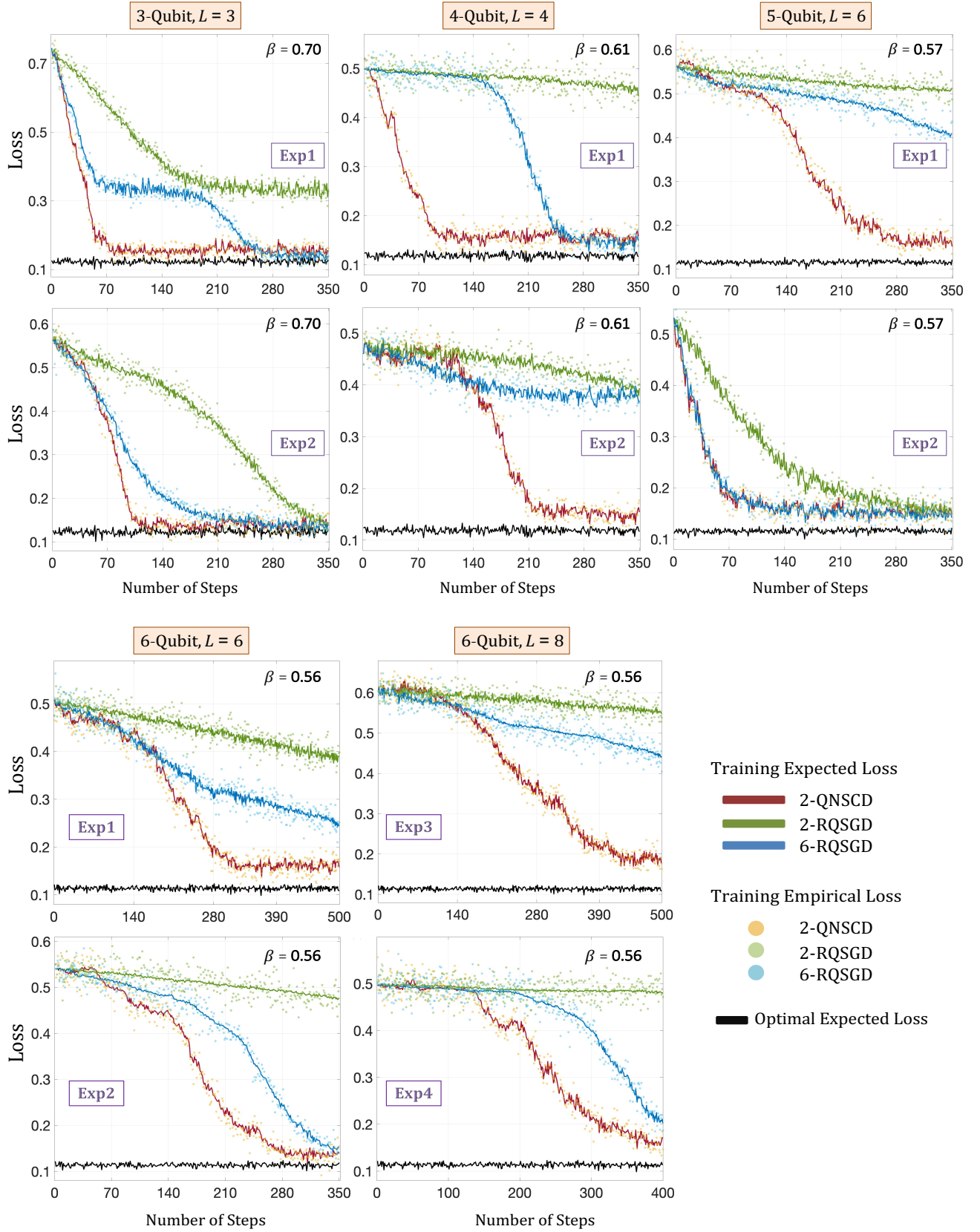


Figure 4: Performance of 2-QNSCD for 3, 4, 5, and 6 qubits. The results demonstrate that 2-QNSCD achieves faster convergence and demonstrates the ability to avoid saddle points and/or barren plateaus effectively.

where the gradient components are almost zero.

For the 5Q case, Exp-1 and Exp-2 correspond to 5Q PQC-1 and 5Q PQC-2, respectively, with different initial points. In 5Q Exp-1, 2-QNSCD shows faster convergence, while in Exp-2, the performance of 6-RQSGD is similar to that of 2-QNSCD. However, it is important to note that 6-RQSGD has higher gate complexity than 2-QNSCD. This is because the gate complexity for E-QFIM estimation is lower than that for gradient estimation. The gate complexity for E-QFIM is, at most, the depth of the PQC, whereas the gradient estimation circuit uses an additional ancilla qubit and a controlled unitary operator, increasing the gate complexity beyond that of the PQC. For the 6Q case, Exp-1 and Exp-2 use 6Q PQC-1, while Exp-3 and Exp-4 use 6Q PQC-2, which has eight layers, all with different initial points. These experiments also demonstrate the advantage of 2-QNSCD over RQSGD-based optimization methods.

Furthermore, we generated a validation set of 1000 samples to test and compare the accuracy of the training methods. The results are summarized in Table I. We note that the accuracy of 2-QNSCD is significantly better than 2-RQSGD and 6-RQSGD, and it is also close to the optimal value computed using (27).

Accuracy	No. of Qubits		2-QNSCD	2-RQSGD	6-RQSGD	Optimal
	3Q	4Q	5Q	6Q	6Q	6Q
Exp-1	84.6 $\pm$ 0.8%	84.6 $\pm$ 1.2%	81.8 $\pm$ 0.8%	83.1 $\pm$ 1.0%	85.9 $\pm$ 1.1%	87.3%
	85.9 $\pm$ 1.1%	84.8 $\pm$ 0.6%	84.0 $\pm$ 1.0%	85.6 $\pm$ 1.2%	85.4 $\pm$ 0.8%	87.6%
Exp-2	85.4 $\pm$ 0.8%	60.8 $\pm$ 1.5%	49.9 $\pm$ 1.3%	52.8 $\pm$ 1.3%	85.6 $\pm$ 0.9%	87.7%
	85.6 $\pm$ 0.9%	61.7 $\pm$ 1.3%	58.7 $\pm$ 1.7%	56.1 $\pm$ 1.4%	84.3 $\pm$ 1.1%	88%
Exp-3	85.1 $\pm$ 0.7%	61.7 $\pm$ 1.3%	58.7 $\pm$ 1.7%	75.6 $\pm$ 1.1%	75.6 $\pm$ 1.1%	
	84.3 $\pm$ 1.1%	84.3 $\pm$ 1.4%	84.3 $\pm$ 1.1%	84.3 $\pm$ 1.4%	84.3 $\pm$ 1.4%	
	80.7 $\pm$ 1.1%	44.7 $\pm$ 1.8%	52.4 $\pm$ 2.2%	56.1 $\pm$ 1.4%	56.1 $\pm$ 1.4%	
	81.4 $\pm$ 1.0%	52.4 $\pm$ 2.2%	52.4 $\pm$ 2.2%	78.5 $\pm$ 1.1%	78.5 $\pm$ 1.1%	

Table I: Accuracy comparison of 2-QNSCD, 2-RQSGD, and 6-RQSGD for different qubit configurations and experimental setups. The last column is the optimal accuracy derived using (27).

## VI. CONVERGENCE ANALYSIS OF QNGD

In this section, we present the convergence analysis of the QNGD with complete access to the metric tensor and gradients. Traditionally, exponential convergence of GD has been proven for a certain class of functions, such as strongly convex functions and the functions that satisfy PL inequality (see Definition 3 below) [Gow18], [KNS16], [Pol63].

**Definition 3** (Polyak-Lojasiewicz (PL) Inequality). A function  $\mathcal{L} : \mathbb{R}^c \rightarrow \mathbb{R}$  is said to satisfy the PL inequality if for all  $\theta \in \mathbb{R}^c$ , the following inequality holds:

$$\frac{1}{2} \|\nabla \mathcal{L}(\theta)\|^2 \geq \mu(\mathcal{L}(\theta) - \mathcal{L}(\theta^*)) \quad \text{for some } \mu > 0, \quad (28)$$

where  $\theta^* \in \mathbb{R}^c$  is a global minimizer for  $\mathcal{L}$ .

However, despite the advantages of NGD over GD, there are limited analytical proofs of convergence that have been established for NGD, for example, for strongly convex loss functions in classical neural networks [Mar20], [ZMG19], whereas almost no formal proof exists within the quantum setup. Therefore, this motivates us to characterize a metric-dependent sufficient condition, *quadratic geometric information* (QGI) inequality, that ensures an exponentially faster rate of convergence.

**Definition 4** (Quadratic Geometric Information (QGI) Inequality). For a given metric tensor  $F$ , a function  $\mathcal{L} : \mathbb{R}^c \rightarrow \mathbb{R}$  is said to satisfy the QGI inequality if the following inequality holds for some  $\mu > 0$  and for all  $\theta \in \mathbb{R}^c$ :

$$\frac{1}{2} \nabla \mathcal{L}^T(\theta) F(\theta)^{-1} \nabla \mathcal{L}(\theta) \geq \mu(\mathcal{L}(\theta) - \mathcal{L}(\theta^*)), \quad (29)$$

where  $\theta^* \in \mathbb{R}^c$  is a global minimizer for  $\mathcal{L}(\theta)$ .

To further understand the significance of the QGI inequality, consider an example from [AD98].

**Example.** Consider the following non-convex loss function using the polar coordinates:

$$\mathcal{L}(r, \theta) = \frac{1}{2} [(r \cos(\theta) - 1)^2 + r^2 \sin^2(\theta)],$$

where  $r \geq 0$  and  $\theta < |\pi|$ . The stationary points of  $\mathcal{L}$  are  $(1, 0)$ ,  $(0, \pi/2)$ , and  $(0, -\pi/2)$  with  $(1, 0)$  being the global minimum. The Riemannian metric tensor for polar coordinates can be written as:

$$F(r, \theta) = \begin{pmatrix} 1 & 0 \\ 0 & r^2 \end{pmatrix}.$$

Clearly, the above loss function does not satisfy the PL inequality because for saddle points  $(0, \pi/2)$  or  $(0, -\pi/2)$ , (28) does not hold for any  $\mu > 0$ . Conversely,  $\mathcal{L}$  satisfies the QGI inequality for all  $(r, \theta) \in [0, \infty) \times (-\pi, -\pi)$  because

$$\lim_{(r, \theta) \rightarrow (0, \pi/2)} \nabla \mathcal{L}(r, \theta)^T F^{-1}(r) \nabla \mathcal{L}(r, \theta) = \lim_{(r, \theta) \rightarrow (0, -\pi/2)} \nabla \mathcal{L}(r, \theta)^T F^{-1}(r) \nabla \mathcal{L}(r, \theta) = 1.$$

This implies if we choose  $\mu \in (0, 1]$ , the QGI inequality holds.

Furthermore, the VQE-inspired loss function, considered as an example in Fig.1, satisfies only QGI inequality (for more details, see Appendix A). This implies that QNGD can provide an exponential rate of convergence when GD fails to do so. Below, we provide the exponential convergence theorem for QNGD under the following assumption:

**Assumption** (L-smooth with respect to a Quadratic Norm [N<sup>+</sup>18]) For a given metric tensor  $F$ , the function  $\mathcal{L}(\theta)$  is L-smooth with respect a quadratic norm  $\|\theta\|_F := (\theta^T F \theta)^{1/2}$ , i.e., for all  $\theta, \theta_1, \theta_2 \in \mathbb{R}^c$ , the following inequalities hold:

$$(a) \quad \mathcal{L}(\theta_2) \leq \mathcal{L}(\theta_1) + \nabla \mathcal{L}(\theta_1)^T (\theta_2 - \theta_1) + \frac{L}{2} \|\theta_2 - \theta_1\|_{F(\theta_1)}, \quad (30)$$

$$(b) \quad \|\nabla \mathcal{L}(\theta)\|_{F(\theta)^{-1}}^2 \leq 2L(\mathcal{L}(\theta) - \mathcal{L}(\theta^*)), \quad (31)$$

for some  $L > 0$ , where  $\theta^*$  is the global minimum of  $\mathcal{L}(\theta)$ .

**Theorem 4** (Convergence of QNGD). *Consider a L-smooth (with respect to  $\|\cdot\|_F$ ) loss function  $\mathcal{L}(\theta)$  that satisfies the QGI inequality (4), for some  $\mu > 0$ . Let  $\theta^* \in \mathbb{R}^c$  be the global minimum of  $\mathcal{L}(\theta)$ . Then, QNGD with a fixed learning rate  $\eta = 1/L$  and the update rule:*

$$\theta^{(t+1)} = \theta^{(t)} - \eta F(\theta^{(t)})^{-1} \nabla \mathcal{L}(\theta^{(t)}),$$

achieves a global exponential convergence rate, given by

$$\mathcal{L}(\theta^{(t)}) - \mathcal{L}(\theta^*) \leq \left(1 - \frac{\mu}{L}\right)^t (\mathcal{L}(\theta^{(0)}) - \mathcal{L}(\theta^*)). \quad (32)$$

*Proof.* We begin with (30) and applying the update rule. Consider the following inequalities:

$$\begin{aligned} \mathcal{L}(\theta^{(t+1)}) &\leq \mathcal{L}(\theta^{(t)}) - \eta \nabla \mathcal{L}(\theta^{(t)})^T F(\theta^{(t)})^{-1} \nabla \mathcal{L}(\theta^{(t)}) + \eta^2 \frac{L}{2} \|F(\theta^{(t)})^{-1} \nabla \mathcal{L}(\theta^{(t)})\|_{F(\theta^{(t)})}^2 \\ &\stackrel{a}{=} \mathcal{L}(\theta^{(t)}) - \frac{1}{2L} \nabla \mathcal{L}(\theta^{(t)})^T F(\theta^{(t)})^{-1} \nabla \mathcal{L}(\theta^{(t)}) \\ &\stackrel{b}{\leq} \mathcal{L}(\theta^{(t)}) - \frac{\mu}{L} (\mathcal{L}(\theta^{(t)}) - \mathcal{L}(\theta^*)), \end{aligned}$$

where (a) follows by putting  $\eta = 1/L$  and from the definition of the quadratic norm, and (b) follows from QGI inequality (4). Thus, after re-arranging and subtracting  $\mathcal{L}(\theta^*)$  from both sides, we get,

$$\mathcal{L}(\theta^{(t+1)}) - \mathcal{L}(\theta^*) \leq \left(1 - \frac{\mu}{L}\right) (\mathcal{L}(\theta^{(t)}) - \mathcal{L}(\theta^*)).$$

Applying this inequality recursively, we get,

$$\mathcal{L}(\theta^{(t)}) - \mathcal{L}(\theta^*) \leq \left(1 - \frac{\mu}{L}\right)^t (\mathcal{L}(\theta^{(0)}) - \mathcal{L}(\theta^*)).$$

Note that from the QGI inequality and (31), we conclude that  $0 < \mu/L < 1$ . This completes the proof of Theorem 4.  $\square$

The proof is notably simple and does not require  $\mathcal{L}$  to be convex or strongly convex. In addition, this is a significant general result for achieving an exponential convergence rate using metric-dependent optimization methods for non-convex problems.

**Acknowledgement:** This work is supported in part by a gift from Accenture and a 2023 QUAD Fellowship and NSF grant CCF-2211423. We thank Touheed Anwar Atif (with Los Alamos National Labs), and Hassan Naseri, Carl Dukatz, and Kung-Chuan Hsu (with Accenture) for the initial discussions on this topic.

## REFERENCES

- [AD98] S. Amari and S.C. Douglas. Why natural gradient? In *Proceedings of the 1998 IEEE International Conference on Acoustics, Speech and Signal Processing, ICASSP '98 (Cat. No.98CH36181)*, volume 2, pages 1213–1216 vol.2, 1998.
- [AJL06] Dorit Aharonov, Vaughan Jones, and Zeph Landau. A polynomial quantum algorithm for approximating the jones polynomial. In *Proceedings of the thirty-eighth annual ACM symposium on Theory of Computing*. ACM, may 2006.
- [Ama98] Shun-Ichi Amari. Natural gradient works efficiently in learning. *Neural computation*, 10(2):251–276, 1998.
- [BBF<sup>+</sup>20] Kerstin Beer, Dmytro Bondarenko, Terry Farrelly, Tobias J. Osborne, Robert Salzmann, Daniel Scheiermann, and Ramona Wolf. Training deep quantum neural networks. *Nature Communications*, 11(1), feb 2020.
- [BC94] Samuel L Braunstein and Carlton M Caves. Statistical distance and the geometry of quantum states. *Physical Review Letters*, 72(22):3439, 1994.
- [BC21] Leonardo Banchi and Gavin E Crooks. Measuring analytic gradients of general quantum evolution with the stochastic parameter shift rule. *Quantum*, 5:386, 2021.
- [BCSC22] Jacob L Beckey, M Cerezo, Akira Sone, and Patrick J Coles. Variational quantum algorithm for estimating the quantum fisher information. *Physical Review Research*, 4(1):013083, 2022.
- [BCvD05] D. Bacon, A.M. Childs, and W. van Dam. From optimal measurement to efficient quantum algorithms for the hidden subgroup problem over semidirect product groups. In *46th Annual IEEE Symposium on Foundations of Computer Science (FOCS'05)*. IEEE, 2005.
- [BCWDW01] Harry Buhrman, Richard Cleve, John Watrous, and Ronald De Wolf. Quantum fingerprinting. *Physical Review Letters*, 87(16):167902, 2001.
- [BIS<sup>+</sup>18] Ville Bergholm, Josh Izaac, Maria Schuld, Christian Gogolin, Shahnawaz Ahmed, Vishnu Ajith, M Sohaib Alam, Guillermo Alonso-Linaje, B AkashNarayanan, Ali Asadi, et al. PennyLane: Automatic differentiation of hybrid quantum-classical computations. *arXiv preprint arXiv:1811.04968*, 2018.
- [BSF94] Yoshua Bengio, Patrice Simard, and Paolo Frasconi. Learning long-term dependencies with gradient descent is difficult. *IEEE transactions on neural networks*, 5(2):157–166, 1994.
- [Bur69] Donald Bures. An extension of kakutani's theorem on infinite product measures to the tensor product of semifinite  $w^*$ -algebras. *Transactions of the American Mathematical Society*, 135:199–212, 1969.
- [BV04] Stephen P Boyd and Lieven Vandenberghe. *Convex optimization*. Cambridge university press, 2004.
- [CEMM98] Richard Cleve, Artur Ekert, Chiara Macchiavello, and Michele Mosca. Quantum algorithms revisited. *Proceedings of the Royal Society of London. Series A: Mathematical, Physical and Engineering Sciences*, 454(1969):339–354, 1998.
- [CWS<sup>+</sup>21] Hongxiang Chen, Leonard Wossnig, Simone Severini, Hartmut Neven, and Masoud Mohseni. Universal discriminative quantum neural networks. *Quantum Machine Intelligence*, 3:1–11, 2021.

[DCH<sup>+</sup>21] Akash V Dixit, Srivatsan Chakram, Kevin He, Ankur Agrawal, Ravi K Naik, David I Schuster, and Aaron Chou. Searching for dark matter with a superconducting qubit. *Physical review letters*, 126(14):141302, 2021.

[DPG<sup>+</sup>14] Yann N Dauphin, Razvan Pascanu, Caglar Gulcehre, Kyunghyun Cho, Surya Ganguli, and Yoshua Bengio. Identifying and attacking the saddle point problem in high-dimensional non-convex optimization. *Advances in neural information processing systems*, 27, 2014.

[DRC17] Christian L Degen, Friedemann Reinhard, and Paola Cappellaro. Quantum sensing. *Reviews of modern physics*, 89(3):035002, 2017.

[EFH<sup>+</sup>22] Andreas Elben, Steven T. Flammia, Hsin-Yuan Huang, Richard Kueng, John Preskill, Benoît Vermersch, and Peter Zoller. The randomized measurement toolbox. *Nature Reviews Physics*, 5(1):9–24, dec 2022.

[FGG14] Edward Farhi, Jeffrey Goldstone, and Sam Gutmann. A quantum approximate optimization algorithm, 2014.

[FGLE12] Steven T Flammia, David Gross, Yi-Kai Liu, and Jens Eisert. Quantum tomography via compressed sensing: error bounds, sample complexity and efficient estimators. *New Journal of Physics*, 14(9):095022, 2012.

[FN18] Edward Farhi and Hartmut Neven. Classification with quantum neural networks on near term processors. *arXiv preprint arXiv:1802.06002*, 2018.

[GB10] Xavier Glorot and Yoshua Bengio. Understanding the difficulty of training deep feedforward neural networks. In *Proceedings of the thirteenth international conference on artificial intelligence and statistics*, pages 249–256. JMLR Workshop and Conference Proceedings, 2010.

[GBC16] Ian Goodfellow, Yoshua Bengio, and Aaron Courville. *Deep learning*. MIT press, 2016.

[GLF<sup>+</sup>10] David Gross, Yi-Kai Liu, Steven T Flammia, Stephen Becker, and Jens Eisert. Quantum state tomography via compressed sensing. *Physical review letters*, 105(15):150401, 2010.

[Gow18] Robert M Gower. Convergence theorems for gradient descent. *Lecture notes for Statistical Optimization*, 2018.

[GR20] Siddhant Garg and Goutham Ramakrishnan. Advances in quantum deep learning: An overview. *arXiv:2005.04316*, May 2020.

[Gro96] Lov K Grover. A fast quantum mechanical algorithm for database search. In *Proceedings of the twenty-eighth annual ACM symposium on Theory of computing*, pages 212–219, 1996.

[GZCW21] Julien Gacon, Christa Zoufal, Giuseppe Carleo, and Stefan Woerner. Simultaneous perturbation stochastic approximation of the quantum fisher information. *Quantum*, 5:567, 2021.

[HCT<sup>+</sup>19] Vojtěch Havlíček, Antonio D Cárcoles, Kristan Temme, Aram W Harrow, Abhinav Kandala, Jerry M Chow, and Jay M Gambetta. Supervised learning with quantum-enhanced feature spaces. *Nature*, 567(7747):209–212, 2019.

[HGS22] Mohsen Heidari, Ananth Grama, and Wojciech Szwankowski. Toward physically realizable quantum neural networks. In *Proceedings of the AAAI Conference on Artificial Intelligence*, volume 36, pages 6902–6909, 2022.

[HHJ<sup>+</sup>16] Jeongwan Haah, Aram W Harrow, Zhengfeng Ji, Xiaodi Wu, and Nengkun Yu. Sample-optimal tomography of quantum states. In *Proceedings of the forty-eighth annual ACM symposium on Theory of Computing*, pages 913–925, 2016.

[HHL09] Aram W Harrow, Avinatan Hassidim, and Seth Lloyd. Quantum algorithm for linear systems of equations. *Physical review letters*, 103(15):150502, 2009.

[HN21] Aram W. Harrow and John C. Napp. Low-depth gradient measurements can improve convergence in variational hybrid quantum-classical algorithms. *Physical Review Letters*, 126(14):140502, apr 2021.

[Hol12] Alexander S. Holevo. *Quantum Systems, Channels, Information*. DE GRUYTER, jan 2012.

[HS10] Alexander Hentschel and Barry C Sanders. Machine learning for precise quantum measurement. *Physical review letters*, 104(6):063603, 2010.

[Hwa03] Won-Young Hwang. Quantum key distribution with high loss: toward global secure communication. *Physical review letters*, 91(5):057901, 2003.

[IPO03] Masato Inoue, Hyeyoung Park, and Masato Okada. On-line learning theory of soft committee machines with correlated hidden units—steepest gradient descent and natural gradient descent—. *Journal of the Physical Society of Japan*, 72(4):805–810, 2003.

[KB22] Balint Koczor and Simon C. Benjamin. Quantum natural gradient generalized to noisy and nonunitary circuits. *Phys. Rev. A*, 106:062416, Dec 2022.

[Kie59] Jack Kiefer. Optimum experimental designs. *Journal of the Royal Statistical Society: Series B (Methodological)*, 21(2):272–304, 1959.

[KMT<sup>+</sup>17] Abhinav Kandala, Antonio Mezzacapo, Kristan Temme, Maika Takita, Markus Brink, Jerry M. Chow, and Jay M. Gambetta. Hardware-efficient variational quantum eigensolver for small molecules and quantum magnets. *Nature*, 549(7671):242–246, sep 2017.

[KNS16] Hamed Karimi, Julie Nutini, and Mark Schmidt. Linear convergence of gradient and proximal-gradient methods under the polyak-ojasiewicz condition. In *Machine Learning and Knowledge Discovery in Databases: European Conference, ECML PKDD 2016, Riva del Garda, Italy, September 2016, Proceedings, Part I* 16, pages 795–811. Springer, 2016.

[Koc21a] Balint Koczor. The dominant eigenvector of a noisy quantum state. *New Journal of Physics*, 23(12):123047, 2021.

[Koc21b] Balint Koczor. Exponential error suppression for near-term quantum devices. *Physical Review X*, 11(3):031057, 2021.

[KW23] Ioannis Kolotouros and Petros Wallden. Random natural gradient. *arXiv preprint arXiv:2311.04135*, 2023.

[LCPLS13] Neil B Lovett, Cecile Crozier, Marti Perarnau-Llobet, and Barry C Sanders. Differential evolution for many-particle adaptive quantum metrology. *Physical review letters*, 110(22):220501, 2013.

[LR18] Nana Liu and Patrick Rebentrost. Quantum machine learning for quantum anomaly detection. *Physical Review A*, 97(4):042315, 2018.

[LXSW14] Jing Liu, Heng-Na Xiong, Fei Song, and Xiaoguang Wang. Fidelity susceptibility and quantum fisher information for density operators with arbitrary ranks. *Physica A: Statistical Mechanics and its Applications*, 410:167–173, 2014.

[LYLW20] Jing Liu, Haidong Yuan, Xiao-Ming Lu, and Xiaoguang Wang. Quantum fisher information matrix and multiparameter estimation. *Journal of Physics A: Mathematical and Theoretical*, 53(2):023001, 2020.

[Mar20] James Martens. New insights and perspectives on the natural gradient method. *Journal of Machine Learning Research*, 21(146):1–76, 2020.

[Mey21] Johannes Jakob Meyer. Fisher information in noisy intermediate-scale quantum applications. *Quantum*, 5:539, 2021.

[MNKF18] K. Mitarai, M. Negoro, M. Kitagawa, and K. Fujii. Quantum circuit learning. *Physical Review A*, 98(3):032309, sep 2018.

[MSB04] Masoud Mohseni, Aephraim M. Steinberg, and Janos A. Bergou. Optical realization of optimal unambiguous discrimination for pure and mixed quantum states. *Physical Review Letters*, 93(20):200403, nov 2004.

[MVAF21] Fabio Valerio Massoli, Lucia Vadicamo, Giuseppe Amato, and Fabrizio Falchi. A leap among entanglement and neural networks: A quantum survey. *arXiv:2107.03313*, July 2021.

[N<sup>+</sup>18] Yurii Nesterov et al. *Lectures on convex optimization*, volume 137. Springer, 2018.

[NC10] Michael A Nielsen and Isaac L Chuang. *Quantum computation and quantum information*. Cambridge university press, 2010.

[Nor11] Kenneth Nordstrom. Convexity of the inverse and moore–penrose inverse. *Linear algebra and its applications*, 434(6):1489–1512, 2011.

[Pet98] Denes Petz. Information-geometry of quantum states. In *Quantum Probability Communications: Volume X*, pages 135–157. World Scientific, 1998.

[PMB13] Razvan Pascanu, Tomas Mikolov, and Yoshua Bengio. On the difficulty of training recurrent neural networks. In *International conference on machine learning*, pages 1310–1318. Pmlr, 2013.

[Pol63] Boris T Polyak. Gradient methods for the minimisation of functionals. *USSR Computational Mathematics and Mathematical Physics*, 3(4):864–878, 1963.

[PS96] Dénes Petz and Csaba Sudár. Geometries of quantum states. *Journal of Mathematical Physics*, 37(6):2662–2673, 1996.

[QZT23] Jun Qi, Xiao-Lei Zhang, and Javier Tejedor. Optimizing quantum federated learning based on federated quantum natural gradient descent. In *ICASSP 2023 - 2023 IEEE International Conference on Acoustics, Speech and Signal Processing (ICASSP)*, pages 1–5, 2023.

[RBMV21] Aniket Rath, Cyril Branciard, Anna Minguzzi, and Benoît Vermersch. Quantum fisher information from randomized measurements. *Physical Review Letters*, 127(26):260501, 2021.

[RSA98] Magnus Rattray, David Saad, and Shun-ichi Amari. Natural gradient descent for on-line learning. *Physical review letters*, 81(24):5461, 1998.

[SBG<sup>+</sup>18] Maria Schuld, Ville Bergholm, Christian Gogolin, Josh Izaac, and Nathan Killoran. Evaluating analytic gradients on quantum hardware. *Phys. Rev. A* 99, 032331 (2019), November 2018.

[SC02] Masahide Sasaki and Alberto Carlini. Quantum learning and universal quantum matching machine. *Physical Review A*, 66(2):022303, 2002.

[SCBC21] Akira Sone, Marco Cerezo, Jacob L Beckey, and Patrick J Coles. Generalized measure of quantum fisher information. *Physical Review A*, 104(6):062602, 2021.

[Sho94] Peter W Shor. Algorithms for quantum computation: discrete logarithms and factoring. In *Proceedings 35th annual symposium on foundations of computer science*, pages 124–134. Ieee, 1994.

[Sho99] Peter W Shor. Polynomial-time algorithms for prime factorization and discrete logarithms on a quantum computer. *SIAM review*, 41(2):303–332, 1999.

[SIKC20] James Stokes, Josh Izaac, Nathan Killoran, and Giuseppe Carleo. Quantum natural gradient. *Quantum*, 4:269, 2020.

[SMMT<sup>+</sup>19] Gael Sentís, Alex Monras, Ramon Muñoz-Tapia, John Calsamiglia, and Emilio Bagan. Unsupervised classification of quantum data. *Physical Review X*, 9(4):041029, 2019.

[SN20] Jun John Sakurai and Jim Napolitano. *Modern quantum mechanics*. Cambridge University Press, 2020.

[SSP14] Maria Schuld, Ilya Sinayskiy, and Francesco Petruccione. The quest for a quantum neural network. *Quantum Information Processing*, 13:2567–2586, 2014.

[SWL<sup>+</sup>17] Sergei Slussarenko, Morgan M Weston, Jun-Gang Li, Nicholas Campbell, Howard M Wiseman, and Geoff J Pryde. Quantum state discrimination using the minimum average number of copies. *Physical review letters*, 118(3):030502, 2017.

[SZ03] Hans-Jürgen Sommers and Karol Zyczkowski. Bures volume of the set of mixed quantum states. *Journal of Physics A: Mathematical and General*, 36(39):10083, 2003.

[Tas20] Hal Tasaki. *Physics and mathematics of quantum many-body systems*, volume 66. Springer, 2020.

[TCC<sup>+</sup>22] Jules Tilly, Hongxiang Chen, Shuxiang Cao, Dario Picozzi, Kanav Setia, Ying Li, Edward Grant, Leonard Wossnig, Ivan Runger, George H Booth, et al. The variational quantum eigensolver: a review of methods and best practices. *Physics Reports*, 986:1–128, 2022.

[TEDMF13] Márcio M Taddei, Bruno M Escher, Luiz Davidovich, and Ruynet L Matos Filho. Quantum speed limit for physical processes. *Physical review letters*, 110(5):050402, 2013.

[TWXL23] Zeyi Tao, Jindi Wu, Qi Xia, and Qun Li. Laws: Look around and warm-start natural gradient descent for quantum neural networks. In *2023 IEEE International Conference on Quantum Software (QSW)*, pages 76–82. IEEE, 2023.

[VRJ<sup>+</sup>23] Vittorio Vitale, Aniket Rath, Petar Jurcevic, Andreas Elben, Cyril Branciard, and Benoît Vermersch. Estimation of the quantum fisher information on a quantum processor. *arXiv preprint arXiv:2307.16882*, 2023.

- [vSK21] Barnaby van Straaten and Balint Koczor. Measurement cost of metric-aware variational quantum algorithms. *PRX Quantum*, 2(3):030324, 2021.
- [WGK20] David Wierichs, Christian Gogolin, and Michael Kastoryano. Avoiding local minima in variational quantum eigensolvers with the natural gradient optimizer. *Physical Review Research*, 2(4):043246, 2020.
- [Wil13] Mark M Wilde. *Quantum information theory*. Cambridge University Press, 2013.
- [WIWL22] David Wierichs, Josh Izaac, Cody Wang, and Cedric Yen-Yu Lin. General parameter-shift rules for quantum gradients. *Quantum*, 6:677, 2022.
- [WXW<sup>+</sup>23] Yizhi Wang, Shichuan Xue, Yaxuan Wang, Jiangfang Ding, Weixu Shi, Dongyang Wang, Yong Liu, Yingwen Liu, Xiang Fu, Guangyao Huang, et al. Experimental quantum natural gradient optimization in photonics. *Optics Letters*, 48(14):3745–3748, 2023.
- [WZ82] William K Wootters and Wojciech H Zurek. A single quantum cannot be cloned. *Nature*, 299(5886):802–803, 1982.
- [XLZZ21] Yi Xia, Wei Li, Quntao Zhuang, and Zheshen Zhang. Quantum-enhanced data classification with a variational entangled sensor network. *Physical Review X*, 11(2):021047, 2021.
- [Yam19] Naoki Yamamoto. On the natural gradient for variational quantum eigensolver. *arXiv preprint arXiv:1909.05074*, 2019.
- [ZMG19] Guodong Zhang, James Martens, and Roger B Grosse. Fast convergence of natural gradient descent for over-parameterized neural networks. *Advances in Neural Information Processing Systems*, 32, 2019.
- [ZZWS17] Zheshen Zhang, Quntao Zhuang, Franco NC Wong, and Jeffrey H Shapiro. Floodlight quantum key distribution: demonstrating a framework for high-rate secure communication. *Physical Review A*, 95(1):012332, 2017.

## APPENDIX

### A. Motivation: Illustrating QNGD convergence.

In this section, we illustrate an advantage of QNGD over GD by presenting a one-qubit VQE-inspired example that satisfies the QGI inequality (Def. 4), whereas it violates the PL inequality (Def. 3). Consider a single-qubit parameterized unitary

$$U(\theta, \phi) := \begin{pmatrix} \cos(\theta/2) & -e^{i\phi} \sin(\theta/2) \\ \sin(\theta/2) & e^{i\phi} \cos(\theta/2) \end{pmatrix},$$

where the parameters' domain is defined as  $\mathcal{R} := \{(\theta, \phi) : 0 \leq \theta < \pi \text{ and } \pi/2 \leq \phi \leq 3\pi/2\}$ . The goal is to optimize the parameters of the state  $|\psi(\theta, \phi)\rangle := U(\theta, \phi) |\psi_0\rangle$ , using QNGD and GD optimization methods, to reach the ground state of the Hamiltonian  $H = \sigma_x$ , starting from the initial state  $|\psi_0\rangle = \left(\frac{|0\rangle + |1\rangle}{\sqrt{2}}\right)$ . The loss function (or energy function) is given as  $\mathcal{L}(\theta, \phi) := \langle \psi(\theta, \phi) | \sigma_x | \psi(\theta, \phi) \rangle = \cos(\theta) \cos(\phi)$ . The stationary points are characterized by  $\nabla \mathcal{L}(\theta, \phi) = 0$  for  $(\theta, \phi) \in \mathcal{R}$ . This gives, a global minimum  $(\theta^*, \phi^*) = (0, \pi)$  and saddle points  $(\pi/2, \pi/2)$  and  $(\pi/2, 3\pi/2)$ . Using Definition 1, the Fubini-Study metric is calculated as:

$$\mathsf{F} = \frac{1}{4} \begin{pmatrix} \cos^2(\phi) & 0 \\ 0 & 1 \end{pmatrix}.$$

We compare the convergence of QNGD and GD against the number of iterations and for a fixed learning rate  $\eta = 0.01$ . In particular, we note the following:

- For all initial points in the region  $\mathcal{R}_1 := \{(\theta_0, \phi_0) \in \mathcal{R} : \theta_0 = \phi_0 \text{ or } \theta_0 + \phi_0 = 2\pi\}$ , GD tends to get trapped at saddle points. This occurs because the steepest descent direction in the Euclidean (or  $\ell_2$ ) geometry, given by  $-\nabla \mathcal{L}$ , guides towards these saddle points for all  $(\theta, \phi) \in \mathcal{R}_1$ . In contrast, QNGD follows a different trajectory, allowing it to avoid these saddle points. Considering the geometry of the space of quantum states, the direction of steepest descent given by  $-\mathbf{F}^{-1} \nabla \mathcal{L}$  tends to bend away from saddle points and converges to the global minimum, as illustrated in Fig. 1(b) and (c).
- Let  $\mathcal{B}_1 := \{(\theta, 3\pi/2) : \theta \in [0, \pi)\}$  and  $\mathcal{B}_2 := \{(\theta, \pi/2) : \theta \in [0, \pi)\}$  denote the top and bottom boundaries of the region  $\mathcal{R}$ , respectively. For all initial points in the region  $\mathcal{R}_2 := \{(\theta_0, \phi_0) \in \mathcal{R} : \theta_0 > \phi_0 \text{ or } \theta_0 + \phi_0 > 2\pi\}$ , GD fails to converge to a global minimum, as shown in Fig. 1(e) and (f). This is because  $-\nabla \mathcal{L}$  directs towards boundaries  $\mathcal{B}_1$  and  $\mathcal{B}_2$ , and thus getting trapped indefinitely. Conversely, QNGD, by following the steepest descent direction in the geometry of the space of quantum states, successfully converges to the global minimum for all  $(\theta_0, \phi_0) \in \mathcal{R}_2$ . This is because the top and bottom boundaries of the region  $\mathcal{R}$  correspond to singular points of the Fubini-Study metric, i.e.,  $\det(\mathbf{F}) = 0$  for all  $(\theta, \phi) \in (\mathcal{B}_1 \cup \mathcal{B}_2)$ .

The quantum states corresponding to the singular region  $\mathcal{B}_1$ , given by  $e^{i\theta/2} \left( \frac{|0\rangle - i|1\rangle}{\sqrt{2}} \right)$ , are indistinguishable, meaning the fidelity between any two quantum states in  $\mathcal{B}_1$  is one. As a result, the loss function remains constant for all parameterized quantum states within  $\mathcal{B}_1$ , irrespective of the Hamiltonian. Similarly, for the singular region  $\mathcal{B}_2$ , the quantum states, given by  $e^{-i\theta/2} \left( \frac{|0\rangle + i|1\rangle}{\sqrt{2}} \right)$ , are also indistinguishable, and loss function remains constant over  $\mathcal{B}_2$  for any Hamiltonian. This implies that for an arbitrary Hamiltonian that leads to a non-constant loss function over  $\mathcal{R}$ , there is a possibility of finding a global (or local) minimum inside  $\mathcal{R}$ . Therefore, the QNGD prevents the parameter trajectory from approaching the boundaries of  $\mathcal{R}$ . In other words, when the parameter trajectory gets near these singular regions, the volume of the metric contracts along the axis corresponding to the parameter  $\theta$ , and the QNGD stretches the descent direction along the same axis and guides it toward the global minimum.

**Convergence using GD:** For all  $(\theta, \phi) \in \mathcal{R}$ , the function  $\mathcal{L}(\theta, \phi)$  does not satisfy the PL inequality for any  $\mu > 0$ . This is because the PL inequality implies that every stationary point is a global minimum. However, when the loss function contains saddle points, this condition fails. For these points, we have  $\|\nabla \mathcal{L}(\theta, \phi)\|^2 = 0$ , but  $(\mathcal{L}(\theta, \phi) - \mathcal{L}(\theta^*, \phi^*)) \neq 0$ . This means that GD fails to guarantee convergence to the global minimum, as illustrated in the example above.

**Convergence using QNGD:** The two saddle points are correctly characterized by the singular points of  $\mathbf{F}$ , i.e.,  $\det(\mathbf{F}(\pi/2, \pi/2)) = \det(\mathbf{F}(\pi/2, 3\pi/2)) = 0$ . Thus, for saddle points, we have

$$\lim_{(\theta, \phi) \rightarrow (\frac{\pi}{2}, \frac{\pi}{2})} \nabla \mathcal{L}(\theta, \phi) \mathbf{F}^{-1}(\phi) \nabla \mathcal{L}(\theta, \phi) = \lim_{(\theta, \phi) \rightarrow (\frac{\pi}{2}, \frac{3\pi}{2})} \nabla \mathcal{L}(\theta, \phi) \mathbf{F}^{-1}(\phi) \nabla \mathcal{L}(\theta, \phi) = 1.$$

This implies if we choose  $\mu \in (0, 1/2]$ , the QGI inequality holds for these points. Therefore, for all  $(\theta, \phi) \in \mathcal{R}$ ,

$\mathcal{L}(\theta, \phi)$  does satisfy the QGI inequality for a sufficiently small  $\mu \in (0, 1/2]$ . This signifies that QNGD can provide an exponential convergence rate to a global minimum even for multi-modal functions with several local-saddle points, particularly encountered in VQAs, whereas GD fails to provide a guaranteed exponential rate of convergence.

### B. Ensemble Distance $d_E$ is Monotonic.

Consider the following ensembles of pure states  $\mathcal{E}_\phi := \{(Q_X(x), |\phi_x\rangle)\}$  and  $\mathcal{E}_\psi := \{(Q_X(x), |\psi_x\rangle)\}$ . The action of the quantum channel  $\mathcal{N}$  on the quantum ensemble of pure states is described using the convex linear postulate of a quantum channel as follows:  $\mathcal{N}(\mathcal{E}_\phi) = \sum_{x \in \mathcal{X}} Q_X(x) \mathcal{N}(|\phi_x\rangle\langle\phi_x|)$ . This implies that a quantum channel acting on an ensemble of pure states produces a density matrix of the form  $\rho^\phi := \sum_x Q_X(x) \rho_x^\phi$ , where  $\rho_x^\phi := \mathcal{N}(|\phi_x\rangle\langle\phi_x|)$ . Similarly,  $\rho^\psi := \sum_x Q_X(x) \rho_x^\psi$ . Therefore, to show that  $d_E$  is monotonic, we need to establish the following

$$d_B(\rho^\phi, \rho^\psi) \leq d_E(\mathcal{E}_\phi, \mathcal{E}_\psi),$$

where  $d_B(\rho^\phi, \rho^\psi)$  is the Bures distance (11) between  $\rho^\phi$  and  $\rho^\psi$ . Consider the following inequalities:

$$\begin{aligned} d_B^2(\rho^\phi, \rho^\psi) &= 2 - 2\sqrt{f_\rho(\rho^\phi, \rho^\psi)} \stackrel{a}{\leq} 2 - 2\sqrt{\sum_x Q_X(x) f_\rho(\rho_x^\phi, \rho_x^\psi)} \stackrel{b}{\leq} 2 - 2\sqrt{\sum_x Q_X(x) |\langle\phi_x|\psi_x\rangle|^2} \\ &\stackrel{c}{\leq} 2 - 2 \left| \sum_x Q_X(x) \langle\phi_x|\psi_x\rangle \right| = d_E^2(\mathcal{E}_\phi, \mathcal{E}_\psi), \end{aligned}$$

where (a) follows from the joint concavity of Uhlmann fidelity [Wil13, Ch.9] and the fact that square root is a monotonically increasing function, (b) follows from the fact that Uhlmann fidelity is monotone with respect to the channel  $\mathcal{N}$ , and (c) follows from the fact that  $|z|^2$  is a convex function, where  $z$  is a complex number, and by using Jensen's inequality. This completes the proof that the Bures distance between the channel outputs is less than or equal to the ensemble distance, thereby showing  $d_E$  is monotonic.

### C. Proof of Theorem 1.

We start the derivation of the E-QFIM by writing the squared ensemble distance between two infinitesimal close ensembles  $\mathcal{E}(\boldsymbol{\theta})$  and  $\mathcal{E}(\boldsymbol{\theta} + d\boldsymbol{\theta})$ , which is given as

$$d_E^2(\mathcal{E}(\boldsymbol{\theta}), \mathcal{E}(\boldsymbol{\theta} + d\boldsymbol{\theta})) = 2 - 2\sqrt{f_E(\boldsymbol{\theta}, \boldsymbol{\theta} + d\boldsymbol{\theta})}. \quad (33)$$

Now, assume  $\boldsymbol{\theta}_i$  denotes parameter corresponds to (a<sup>th</sup> layer, p<sup>th</sup> qubit), and  $\boldsymbol{\theta}_j$  denotes parameter corresponds to (b<sup>th</sup> layer, q<sup>th</sup> qubit). Then, the Taylor series of  $|\phi(\boldsymbol{\theta} + d\boldsymbol{\theta})\rangle$  (up to the first order) is written as:

$$|\phi(\boldsymbol{\theta} + d\boldsymbol{\theta})\rangle = |\phi(\boldsymbol{\theta})\rangle + \sum_{i=1}^c |\partial_i \phi(\boldsymbol{\theta})\rangle d\boldsymbol{\theta}_i.$$

Therefore, we can write the fidelity between  $\mathcal{E}(\boldsymbol{\theta})$  and  $\mathcal{E}(\boldsymbol{\theta} + d\boldsymbol{\theta})$  as:

$$\begin{aligned} f_{\mathcal{E}}(\boldsymbol{\theta}, \boldsymbol{\theta} + d\boldsymbol{\theta}) &= \left| \sum_{x \in \mathcal{X}} Q_X(x) \left( \langle \phi_x(\boldsymbol{\theta}) | \phi_x(\boldsymbol{\theta}) \rangle + \sum_{i=1}^c d\boldsymbol{\theta}_i \langle \phi_x(\boldsymbol{\theta}) | \partial_i \phi_x(\boldsymbol{\theta}) \rangle \right) \right|^2 \\ &= 1 + \sum_{x \in \mathcal{X}} Q_X(x) \sum_{i=1}^c d\boldsymbol{\theta}_i \left( \langle \phi_x(\boldsymbol{\theta}) | \partial_i \phi_x(\boldsymbol{\theta}) \rangle + \langle \partial_i \phi_x(\boldsymbol{\theta}) | \phi_x(\boldsymbol{\theta}) \rangle \right) \\ &\quad + \sum_{x_1 x_2} Q_X(x_1) Q_X(x_2) \sum_{ij} d\boldsymbol{\theta}_i d\boldsymbol{\theta}_j \langle \partial_i \phi_{x_1}(\boldsymbol{\theta}) | \phi_{x_1}(\boldsymbol{\theta}) \rangle \langle \phi_{x_2}(\boldsymbol{\theta}) | \partial_j \phi_{x_2}(\boldsymbol{\theta}) \rangle. \end{aligned} \quad (34)$$

Using  $f_{\mathcal{E}}(\boldsymbol{\theta} + d\boldsymbol{\theta}, \boldsymbol{\theta} + d\boldsymbol{\theta}) = 1$ , we obtain

$$\begin{aligned} \left| \sum_{x \in \mathcal{X}} Q_X(x) \langle \phi_x(\boldsymbol{\theta} + d\boldsymbol{\theta}) | \phi_x(\boldsymbol{\theta} + d\boldsymbol{\theta}) \rangle \right| &= \left| \sum_{x \in \mathcal{X}} Q_X(x) \left[ 1 + \sum_i d\boldsymbol{\theta}_i (\langle \phi_x(\boldsymbol{\theta}) | \partial_i \phi_x(\boldsymbol{\theta}) \rangle + \langle \partial_i \phi_x(\boldsymbol{\theta}) | \phi_x(\boldsymbol{\theta}) \rangle) \right. \right. \\ &\quad \left. \left. + \sum_{ij} d\boldsymbol{\theta}_i d\boldsymbol{\theta}_j \langle \partial_i \phi_x(\boldsymbol{\theta}) | \partial_j \phi_x(\boldsymbol{\theta}) \rangle \right] \right| = 1. \end{aligned} \quad (35)$$

The above equality implies the following relation:

$$\sum_i d\boldsymbol{\theta}_i (\langle \phi_x(\boldsymbol{\theta}) | \partial_i \phi_x(\boldsymbol{\theta}) \rangle + \langle \partial_i \phi_x(\boldsymbol{\theta}) | \phi_x(\boldsymbol{\theta}) \rangle) = - \sum_{ij} d\boldsymbol{\theta}_i d\boldsymbol{\theta}_j \langle \partial_i \phi_x(\boldsymbol{\theta}) | \partial_j \phi_x(\boldsymbol{\theta}) \rangle. \quad (36)$$

Finally, considering (33), (34), and (36) collectively, we see that

$$\begin{aligned} \mathcal{F}_{(i,j)}^{\mathcal{E}}(\boldsymbol{\theta}) &= \frac{1}{2} \frac{\partial^2}{\partial d\boldsymbol{\theta}_i \partial d\boldsymbol{\theta}_j} d_{\mathcal{E}}^2(\boldsymbol{\theta}, \boldsymbol{\theta} + d\boldsymbol{\theta}) \Big|_{d\boldsymbol{\theta}=0} \\ &= \frac{1}{2} \frac{\partial^2}{\partial d\boldsymbol{\theta}_i \partial d\boldsymbol{\theta}_j} \left[ 2 - 2 \left( 1 - \sum_{x \in \mathcal{X}} Q_X(x) \sum_{ij} d\boldsymbol{\theta}_i d\boldsymbol{\theta}_j \langle \partial_i \phi_x(\boldsymbol{\theta}) | \partial_j \phi_x(\boldsymbol{\theta}) \rangle \right. \right. \\ &\quad \left. \left. + \sum_{x_1 x_2} Q_X(x_1) Q_X(x_2) \sum_{ij} d\boldsymbol{\theta}_i d\boldsymbol{\theta}_j \langle \partial_i \phi_{x_1}(\boldsymbol{\theta}) | \phi_{x_1}(\boldsymbol{\theta}) \rangle \langle \phi_{x_2}(\boldsymbol{\theta}) | \partial_j \phi_{x_2}(\boldsymbol{\theta}) \rangle \right)^{1/2} \right] \Big|_{d\boldsymbol{\theta}=0} \\ &\stackrel{a}{=} \text{Re} \left\{ \sum_{x \in \mathcal{X}} Q_X(x) \langle \partial_i \phi_x(\boldsymbol{\theta}) | \partial_j \phi_x(\boldsymbol{\theta}) \rangle - \sum_{x_1 x_2} Q_X(x_1) Q_X(x_2) \langle \partial_i \phi_{x_1}(\boldsymbol{\theta}) | \phi_{x_1}(\boldsymbol{\theta}) \rangle \langle \phi_{x_2}(\boldsymbol{\theta}) | \partial_j \phi_{x_2}(\boldsymbol{\theta}) \rangle \right\} \\ &\stackrel{b}{=} \text{Re} \left\{ \text{Tr} \left( \frac{\partial U^\dagger(\boldsymbol{\theta})}{\partial \boldsymbol{\theta}_i} \frac{\partial U(\boldsymbol{\theta})}{\partial \boldsymbol{\theta}_j} \rho \right) - \text{Tr} \left( \frac{\partial U^\dagger(\boldsymbol{\theta})}{\partial \boldsymbol{\theta}_i} U(\boldsymbol{\theta}) \rho \right) \text{Tr} \left( U^\dagger(\boldsymbol{\theta}) \frac{\partial U(\boldsymbol{\theta})}{\partial \boldsymbol{\theta}_j} \rho \right) \right\} \\ &= \text{Re} \{ \text{Tr}(\Upsilon_i(\boldsymbol{\theta}) \Upsilon_j(\boldsymbol{\theta}) \rho) - \text{Tr}(\Upsilon_i(\boldsymbol{\theta}) \rho) \text{Tr}(\Upsilon_j(\boldsymbol{\theta}) \rho) \}, \end{aligned} \quad (37)$$

where in (a), the real part appears from the fact that  $d\boldsymbol{\theta}_i d\boldsymbol{\theta}_j$  occurs twice in the summation but with the conjugated terms and (b) follows from the cyclicity of trace. This completes the proof of Theorem 1.

#### D. Derivation of the $\mathcal{F}^E$ expression for the QNN Model discussed in Section II.

Consider the parameterized unitary of the  $a^{\text{th}}$  hidden layer,  $U_a(\boldsymbol{\theta}_a) = \bigotimes_{p=1}^d R_{\sigma_p^a}(\boldsymbol{\theta}_{(a,p)})$ . Recalling the notation from Sec. II, the derivative of  $W_a(\boldsymbol{\theta}_a)$  with respect to  $p^{\text{th}}$  qubit parameter can be expressed as:

$$\partial_{a_p} W_a(\boldsymbol{\theta}_a) := \frac{\partial W_a(\boldsymbol{\theta}_a)}{\partial \boldsymbol{\theta}_{(a,p)}} = -\frac{i}{2} W_a(\boldsymbol{\theta}_a) (\mathbb{I}^{\otimes[1:p]} \otimes \sigma_p^a \otimes \mathbb{I}^{\otimes(p:d)}).$$

Further, the derivative of  $U(\boldsymbol{\theta})$  can be written as:

$$\partial_{a_p} U(\boldsymbol{\theta}) := \frac{\partial U(\boldsymbol{\theta})}{\partial \boldsymbol{\theta}_{(a,p)}} = -\frac{i}{2} W_{[L:a]} (\mathbb{I}^{\otimes[1:p]} \otimes \sigma_p^a \otimes \mathbb{I}^{\otimes(p:d)}) W_{(a:1]}, \quad (38)$$

Using (38), we compute the elements of the E-QFIM corresponding to the ( $a^{\text{th}}$  layer,  $p^{\text{th}}$  qubit) parameter and ( $b^{\text{th}}$  layer,  $q^{\text{th}}$  qubit) parameter. Consider the second term of  $\mathcal{F}^E$  (see (15)).

$$\begin{aligned} & \text{Tr}\{(\partial_{a_p} U^\dagger(\boldsymbol{\theta})) U(\boldsymbol{\theta}) \rho\} \text{Tr}\{U^\dagger(\boldsymbol{\theta})(\partial_{b_q} U(\boldsymbol{\theta})) \rho\} \\ &= 0.25 \cdot \text{Tr}\{W_{[1:a]}^\dagger (\mathbb{I}^{\otimes[1:p]} \otimes \sigma_p^a \otimes \mathbb{I}^{\otimes(p:d)}) W_{[a:L]}^\dagger W_{[L:1]} \rho\} \text{Tr}\{W_{[1:L]}^\dagger W_{[L:b]} (\mathbb{I}^{\otimes[1:q]} \otimes \sigma_q^b \otimes \mathbb{I}^{\otimes(q:d)}) W_{(b:1]} \rho\} \\ &= 0.25 \cdot \text{Tr}\{W_{[1:a]}^\dagger (\mathbb{I}^{\otimes[1:p]} \otimes \sigma_p^a \otimes \mathbb{I}^{\otimes(p:d)}) W_{(a:1]} \rho\} \text{Tr}\{W_{[1:b]}^\dagger (\mathbb{I}^{\otimes[1:q]} \otimes \sigma_q^b \otimes \mathbb{I}^{\otimes(q:d)}) W_{(b:1]} \rho\} \\ &= \text{Tr}\{G_{a_p} \rho\} \text{Tr}\{G_{b_q} \rho\}. \end{aligned} \quad (39)$$

To compute the first term of (15), without loss of generality, assume  $a \leq b$ . Thus, we get

$$\begin{aligned} & \text{Re}\left\{ \text{Tr}((\partial_{a_p} U^\dagger(\boldsymbol{\theta}))(\partial_{b_q} U(\boldsymbol{\theta})) \rho) \right\} \\ &= 0.25 \cdot \text{Re}\left\{ \text{Tr}(W_{[1:a]}^\dagger (\mathbb{I}^{\otimes[1:p]} \otimes \sigma_p^a \otimes \mathbb{I}^{\otimes(p:d)}) W_{[a:b]}^\dagger (\mathbb{I}^{\otimes[1:q]} \otimes \sigma_q^b \otimes \mathbb{I}^{\otimes(q:d)}) W_{(b:1]} \rho) \right\} \\ &= 0.25 \cdot \text{Re}\left\{ \text{Tr}(W_{[1:a]}^\dagger (\mathbb{I}^{\otimes[1:p]} \otimes \sigma_p^a \otimes \mathbb{I}^{\otimes(p:d)}) W_{(a:1]} W_{[1:b]}^\dagger (\mathbb{I}^{\otimes[1:q]} \otimes \sigma_q^b \otimes \mathbb{I}^{\otimes(q:d)}) W_{(b:1]} \rho) \right\} \\ &= \text{Re}\{\text{Tr}(G_{a_p} G_{b_q} \rho)\} = \frac{1}{2} \text{Tr}(\{G_{a_p}, G_{b_q}\} \rho), \end{aligned} \quad (40)$$

where the last equality follows from the cyclicity of the trace. Combining these expressions, the E-QFIM takes the form:  $\mathcal{F}_{(a_p, b_q)}(\boldsymbol{\theta}) = \text{Cov}(G_{a_p}, G_{b_q})_\rho$ .

#### E. Proof of Lemma 2.

Using the cyclicity of trace, we rewrite the expectation of  $\{\mathbf{A}, \mathbf{B}\}$  with respect to the state  $|\phi\rangle$  as follows:

$$\langle \phi | \{\mathbf{A}, \mathbf{B}\} | \phi \rangle = \text{Tr}(\{\mathbf{A}, \mathbf{B}\} \Phi) = \text{Tr}(\mathbf{B} \Phi \mathbf{A} + \mathbf{B} \mathbf{A} \Phi) = \text{Tr}(\{\mathbf{A}, \Phi\} \mathbf{B}). \quad (41)$$

Suppose  $A$  is a random variable denoting the measurement outcome of  $\mathcal{M} = \{\mathbf{A}_+, \mathbf{A}_-\}$  on the state  $|\phi\rangle$ . The probability of obtaining outcome 1, i.e.,  $\mathbb{P}\{A = 1\} = \text{Tr}(\mathbf{A}_+ \Phi)$ . Similarly,  $\mathbb{P}\{A = -1\} = \text{Tr}(\mathbf{A}_- \Phi)$ . Then,

we decompose the anit-commutator  $\{\mathbf{A}, \Phi\}$  in terms of  $\mathbf{A}_+$  and  $\mathbf{A}_-$  as follows:

$$\begin{aligned}\{\mathbf{A}, \Phi\} &= \mathbf{A}\Phi I + I\Phi\mathbf{A} \stackrel{a}{=} (\mathbf{A}_+ - \mathbf{A}_-)\Phi(\mathbf{A}_+ + \mathbf{A}_-) + (\mathbf{A}_+ + \mathbf{A}_-)\Phi(\mathbf{A}_+ - \mathbf{A}_-) \\ &= 2[\mathbf{A}_+\Phi\mathbf{A}_+ - \mathbf{A}_-\Phi\mathbf{A}_-] \\ &= 2[\mathbb{P}\{A = 1\}\Phi(\mathbf{A}_+) - \mathbb{P}\{A = -1\}\Phi(\mathbf{A}_-)],\end{aligned}$$

where (a) follows from the facts that the Hermitian matrix has orthonormal eigenvectors for distinct eigenvalues and  $\mathbf{A}^2 = \mathbb{I}$ . Here,  $\Phi(\mathbf{A}_+)$  and  $\Phi(\mathbf{A}_-)$  denote the post-measurement state when we measure outcomes  $+1$  and  $-1$ , respectively. Subsequently, let  $B$  be the random variable denoting the measurement outcome of the post-measurement state along the eigenvectors of  $\mathbf{B}$ . Then,

$$\begin{aligned}\frac{1}{2}\text{Tr}(\{\mathbf{A}, \Phi\}\mathbf{B}) &= \mathbb{P}\{A = 1\}\text{Tr}(\mathbf{B}\Phi(\mathbf{A}_+)) - \mathbb{P}\{A = -1\}\text{Tr}(\mathbf{B}\Phi(\mathbf{A}_-)) \\ &= \mathbb{P}\{A = 1\}\mathbb{E}[AB|A = 1] + \mathbb{P}\{A = -1\}\mathbb{E}[AB|A = -1] = \mathbb{E}[AB].\end{aligned}\quad (42)$$

Hence, from (41) and (42), we get  $\langle\phi|\{\mathbf{A}, \mathbf{B}\}|\phi\rangle = 2 \cdot \mathbb{E}[AB]$ . This completes the proof of Lemma 2.

#### F. Proof of Lemma 3.

Let  $|\phi_x^a\rangle := W_{(a:1)}|\phi_x\rangle$  denote the input state to the  $a^{\text{th}}$  layer of the PQC. We denote  $\Sigma_p^a := (\mathbb{I}^{\otimes[1:p]} \otimes \sigma_p^a \otimes \mathbb{I}^{\otimes(p:d)})$  and  $\Sigma_q^b := (\mathbb{I}^{\otimes[1:q]} \otimes \sigma_q^b \otimes \mathbb{I}^{\otimes(q:d)})$ . We first compute the expectation of diagonal entries. Observe that  $\mathbb{E}[v_i||\phi_{x_i}\rangle] = \text{Tr}(\Sigma_q^b \Phi_{x_i}^b)$  for  $i = 1, 2$ . For  $z_{22}$ ,

$$\begin{aligned}\mathbb{E}[z_{22}] &= \mathbb{E}[0.25 \cdot (1 - v_1 v_2)] \stackrel{a}{=} 0.25 \cdot (1 - \mathbb{E}_{X_1}[\mathbb{E}[v_1||\phi_{x_1}\rangle]]\mathbb{E}_{X_2}[\mathbb{E}[v_2||\phi_{x_2}\rangle]]) \\ &= 0.25 \cdot (1 - \mathbb{E}_{X_1}[\text{Tr}(\Sigma_q^b \Phi_{x_1}^b)]\mathbb{E}_{X_2}[\text{Tr}(\Sigma_q^b \Phi_{x_2}^b)]) \\ &= 0.25 - 0.25[\text{Tr}(\Sigma_q^b W_{(b:1)}\rho W_{(1:b)}^\dagger)]^2 = 0.25 - [\text{Tr}(G_{b_q}\rho)]^2,\end{aligned}$$

where (a) follows because  $|\phi_{x_1}\rangle$  and  $|\phi_{x_2}\rangle$  are i.i.d. samples. This gives the desired result for  $z_{22}$ . Next, we note that the structure of the pair  $(v_1, v_2)$  is exactly the same as that of  $(u_1, u_2)$  with the correspondence  $a_p \leftrightarrow b_q$ . Hence, for  $z_{11} = 0.25 \cdot (1 - u_1 u_2)$ , we get  $\mathbb{E}[z_{11}] = 0.25 - \text{Tr}(G_{a_p}\rho)^2$ .

Finally, we compute the expectation of off-diagonal entries. Recall the definition of Hermitian operators  $G_{a_p}$  and  $G_{b_q}$ , then consider the following set of equalities:

$$\begin{aligned}\{G_{a_p}, G_{b_q}\} &= G_{a_p}G_{b_q} + G_{b_q}G_{a_p} \\ &= 0.25 \cdot (W_{[1:a]}^\dagger \Sigma_p^a W_{(a:1)} W_{[1:b]}^\dagger \Sigma_q^b W_{(b:1)} + W_{[1:b]}^\dagger \Sigma_q^b W_{(b:1)} W_{[1:a]}^\dagger \Sigma_p^a W_{(a:1)}) \\ &= 0.25 \cdot (W_{[1:a]}^\dagger \Sigma_p^a W_{[a:b]}^\dagger \Sigma_q^b W_{(b:1)} + W_{[1:b]}^\dagger \Sigma_q^b W_{(b:a)}^\dagger \Sigma_p^a W_{(a:1)}).\end{aligned}$$

Using the above expansion of  $\{G_{a_p}, G_{b_q}\}$  and cyclicity of trace, we get

$$\begin{aligned}
\langle \phi_x | \{G_{a_p}, G_{b_q}\} | \phi_x \rangle &= \text{Tr}(\{G_{a_p}, G_{b_q}\} \Phi_x) \\
&= 0.25 \cdot \text{Tr}(\Sigma_p^a W_{[a:b]}^\dagger \Sigma_q^b W_{(b:1]} \Phi_x W_{[1:a]}^\dagger) + \text{Tr}(\Sigma_q^b W_{(b:a]} \Sigma_p^a W_{(a:1]} \Phi_x W_{[1:b]}^\dagger) \\
&\stackrel{a}{=} 0.25 \cdot \text{Tr}(\Sigma_p^a W_{[a:b]}^\dagger \Sigma_q^b W_{(b:a]} \Phi_x^a) + \text{Tr}(\Sigma_q^b W_{(b:a]} \Sigma_p^a \Phi_x^a W_{[a:b]}^\dagger) \\
&= 0.25 \cdot \text{Tr}(\Sigma_q^b W_{(b:a]} \Phi_x^a \Sigma_p^a W_{[a:b]}^\dagger) + \text{Tr}(\Sigma_q^b W_{(b:a]} \Sigma_p^a \Phi_x^a W_{[a:b]}^\dagger) \\
&= 0.25 \cdot \text{Tr}(\Sigma_q^b W_{(b:a]} \{\Sigma_p^a, \Phi_x^a\} W_{[a:b]}^\dagger), \tag{43}
\end{aligned}$$

where (a) follows from the definition  $\Phi_x^a$ . Using the following facts: (i)  $\Sigma_p^a$  is Hermitian, (ii)  $(\Sigma_p^a)^2 = \mathbb{I}$ , (iii)  $\text{Tr}(\{\mathbf{A}, \mathbf{B}\} \Phi) = \text{Tr}(\mathbf{B}\{\mathbf{A}, \Phi\})$ , and Lemma 2, we can write

$$\mathbb{E}[u_i w_i | |\phi_{x_{i+2}}\rangle] = 0.5 \cdot \text{Tr}(W_{[a:b]}^\dagger \Sigma_q^b W_{(b:a]} \{\Sigma_p^a, \Phi_{x_{i+2}}^a\}), \tag{44}$$

for  $i = 1, 2$ , where we used the Heisenberg picture of quantum measurements:  $\text{Tr}(\Lambda U \rho U^\dagger) = \text{Tr}(U^\dagger \Lambda U \rho)$ , where  $\Lambda$  and  $U$  represent a measurement and unitary operator, respectively [SN20]. Now, we are equipped to compute the expectation of the off-diagonal entries. For  $z_{12} = z_{21}$ ,

$$\begin{aligned}
\mathbb{E}[z_{12}] &= 0.125 \cdot \mathbb{E}[u_1 w_1 + u_2 w_2] - 0.0625 \cdot \mathbb{E}[(u_1 + u_2)(v_1 + v_2)] \\
&\stackrel{a}{=} 0.125 \cdot (\mathbb{E}_{X_3}[\mathbb{E}[u_1 w_1 | |\phi_{x_3}\rangle]] + \mathbb{E}_{X_4}[\mathbb{E}[u_2 w_2 | |\phi_{x_4}\rangle]]) - \text{Tr}(G_{a_p} \rho) \text{Tr}(G_{b_q} \rho) \\
&\stackrel{b}{=} 0.0625 \cdot (\mathbb{E}_{X_3}[\text{Tr}(\Sigma_q^b W_{(b:a]} \{\Sigma_p^a, \Phi_{x_3}^a\} W_{[a:b]}^\dagger)] + \mathbb{E}_{X_4}[\text{Tr}(\Sigma_q^b W_{(b:a]} \{\Sigma_p^a, \Phi_{x_4}^a\} W_{[a:b]}^\dagger)]) \\
&\quad - \text{Tr}(G_{a_p} \rho) \text{Tr}(G_{b_q} \rho) \\
&\stackrel{c}{=} 0.125 \cdot \text{Tr}(\Sigma_q^b W_{(b:a]} \{\Sigma_p^a, \rho^a\} W_{[a:b]}^\dagger) - \text{Tr}(G_{a_p} \rho) \text{Tr}(G_{b_q} \rho) \\
&\stackrel{d}{=} 0.5 \cdot \text{Tr}(\{G_{a_p}, G_{b_q}\} \rho) - \text{Tr}(G_{a_p} \rho) \text{Tr}(G_{b_q} \rho),
\end{aligned}$$

where (a) follows because  $|\phi_{x_1}\rangle, |\phi_{x_2}\rangle, |\phi_{x_3}\rangle$ , and  $|\phi_{x_4}\rangle$  are i.i.d. samples and the analysis of  $z_{11}, z_{22}$ , (b) follows from (44), (c) follows by defining  $\rho^a := W_{(a:1]} \rho W_{[1:a]}^\dagger$ , and (d) follows from (43). This completes the proof of Lemma 3.

#### G. Proof of Theorem 2.

Without loss of generality, assume  $a \leq b$ . Consider the following equalities:

$$\mathbb{E}[\bar{\mathbf{Z}}(a_p, b_q)] = \frac{c(c-1)}{2} \mathbb{E} \left[ \tilde{\mathbf{Z}}(a_p, b_q) - \frac{2\beta}{c} \mathbb{I} \right] \stackrel{a}{=} \frac{1}{2} \sum_{a_p \neq b_q} \mathbb{E} \left[ \tilde{\mathbf{Z}}(a_p, b_q) \right] - (c-1)\beta \mathbb{I}$$

$$\begin{aligned}
& \stackrel{b}{=} \frac{1}{2} \sum_{a_p \neq b_q} \begin{bmatrix} 0 & & & & & \\ & \ddots & & & & \\ & & 0 & & & \\ & & & \frac{1}{(c-1)} \mathcal{F}_{(a_p, a_p)}^{\mathcal{E}} + \beta & 0 & \dots & 0 & \mathcal{F}_{(a_p, b_q)}^{\mathcal{E}} \\ & & & 0 & 0 & \dots & 0 & 0 \\ & & & \vdots & \vdots & \ddots & \vdots & \vdots \\ & & & 0 & 0 & \dots & 0 & 0 \\ & & & \mathcal{F}_{(b_q, a_p)}^{\mathcal{E}} & 0 & \dots & 0 & \frac{1}{(c-1)} \mathcal{F}_{(b_q, b_q)}^{\mathcal{E}} + \beta \\ & & & & & & & 0 \\ & & & & & & & \ddots \\ & & & & & & & 0 \end{bmatrix} - (c-1)\beta \mathbb{I} \\
& \stackrel{c}{=} \frac{1}{2} (2\mathcal{F}^{\mathcal{E}} + 2(c-1)\beta \mathbb{I}) - (c-1)\beta \mathbb{I} = \mathcal{F}^{\mathcal{E}},
\end{aligned}$$

where (a) follows by taking the expectation over the random pair of coordinates  $(a_p, b_q)$ , (b) follows from Lemma 3, and (c) follows by expanding the summation and noting the following arguments. The non-zero off-diagonal terms arise in the summation only twice, whereas the non-zero diagonal terms appear in the summation  $2(c-1)$  times. This completes the proof of Theorem 2.

#### H. Derivation of the Gradient of Per-Sample Expected Loss.

Recall, from (38), the derivative of  $U(\boldsymbol{\theta})$  with respect to the  $(a^{\text{th}} \text{ layer}, p^{\text{th}} \text{ qubit})$  parameter  $\theta_{(a,p)}$  is given as:

$$\partial_{a_p} U(\boldsymbol{\theta}) := \frac{\partial U(\boldsymbol{\theta})}{\partial \theta_{(a,p)}} = -\frac{i}{2} W_{[L:a]} \Sigma_p^a W_{(a:1)}.$$

Using the above derivative, compute the following expression:

$$\begin{aligned}
(\partial_{a_p} U(\boldsymbol{\theta})) \Phi_x U^\dagger(\boldsymbol{\theta}) + U(\boldsymbol{\theta}) \Phi_x (\partial_{a_p} U^\dagger(\boldsymbol{\theta})) &= -\frac{i}{2} W_{[L:a]} \Sigma_p^a \Phi_x^a W_{[a:L]}^\dagger + \frac{i}{2} W_{[L:a]} \Phi_x^a \Sigma_p^a W_{[a:L]}^\dagger \\
&= -\frac{i}{2} W_{[L:a]} [\Sigma_p^a, \Phi_x^a] W_{[a:L]}^\dagger.
\end{aligned} \tag{45}$$

Thus, using (45), the gradient of per-sample expected loss can be written as:

$$\begin{aligned}
\frac{\partial \mathcal{L}(\boldsymbol{\theta}, |\phi\rangle, y)}{\partial \theta_{(a,p)}} &= \sum_{\hat{y} \in \mathcal{Y}} \ell(y, \hat{y}) \text{Tr}\{\Lambda_{\hat{y}}((\partial_{a_p} U(\boldsymbol{\theta})) \Phi U^\dagger(\boldsymbol{\theta}) + U(\boldsymbol{\theta}) \Phi (\partial_{a_p} U^\dagger(\boldsymbol{\theta})))\} \\
&= \sum_{\hat{y} \in \mathcal{Y}} -\frac{i}{2} \ell(y, \hat{y}) \text{Tr}\{\Lambda_{\hat{y}} W_{[L:a]} [\Sigma_p^a, \Phi_x^a] W_{[a:L]}^\dagger\}.
\end{aligned} \tag{46}$$

This completes the derivation.

#### I. Proof of Lemma 4.

We first prove the following lemma.

**Lemma 5.** Consider a Hermitian operator  $\mathbf{A}$  on  $\mathcal{H}^d$ , such that  $\mathbf{A}^2 = \mathbb{I}$ . Then, for any operator  $\Phi$  on  $\mathcal{H}^d$  the following holds:

$$[\mathbf{A}, \Phi] = i(e^{-i\pi\mathbf{A}/4} \Phi e^{i\pi\mathbf{A}/4} - e^{i\pi\mathbf{A}/4} \Phi e^{-i\pi\mathbf{A}/4}).$$

*Proof.* The proof follows from [MNKF18]. However, for convenience, we provide a succinct proof below. With the definition of  $\mathbf{A}$ , note that  $\mathbf{A}^2 = \mathbb{I}$ . Therefore, using Taylor expansion, we have,

$$e^{i\beta\mathbf{A}} = \cos(\beta)\mathbb{I} + i\sin(\beta)\mathbf{A} \quad \text{for all } \beta \in [0, 2\pi).$$

Next, we simplify the following expression:

$$i(e^{-i\pi\mathbf{A}/4} \Phi e^{i\pi\mathbf{A}/4} - e^{i\pi\mathbf{A}/4} \Phi e^{-i\pi\mathbf{A}/4}) = \frac{i}{2}((\mathbb{I} - i\mathbf{A})\Phi(\mathbb{I} + i\mathbf{A}) - (\mathbb{I} + i\mathbf{A})\Phi(\mathbb{I} - i\mathbf{A})) = [\mathbf{A}, \Phi].$$

This completes the proof of Lemma 5.  $\square$

With the intention of employing the above lemma and considering the definition of  $\mathbf{V}$ , we have

$$\begin{aligned} \mathbf{V}(\Phi \otimes |+\rangle\langle+|)\mathbf{V}^\dagger &= \frac{1}{2}(e^{i\pi\mathbf{A}/4} \Phi e^{-i\pi\mathbf{A}/4} \otimes |0\rangle\langle 0| + e^{i\pi\mathbf{A}/4} \Phi e^{i\pi\mathbf{A}/4} \otimes |0\rangle\langle 1| \\ &\quad + e^{-i\pi\mathbf{A}/4} \Phi e^{-i\pi\mathbf{A}/4} \otimes |1\rangle\langle 0| + e^{-i\pi\mathbf{A}/4} \Phi e^{i\pi\mathbf{A}/4} \otimes |1\rangle\langle 1|). \end{aligned}$$

Next, using the above expression, we compute the following expectation:

$$\begin{aligned} 2i\langle\tilde{\phi}|\mathbf{V}^\dagger O\mathbf{V}|\tilde{\phi}\rangle &= 2i\text{Tr}\{O\mathbf{V}\tilde{\Phi}\mathbf{V}^\dagger\} = i(\text{Tr}\{\mathbf{B}e^{i\pi\mathbf{A}/4} \Phi e^{-i\pi\mathbf{A}/4} - \mathbf{B}e^{-i\pi\mathbf{A}/4} \Phi e^{i\pi\mathbf{A}/4}\}) \\ &\stackrel{a}{=} \text{Tr}\{\mathbf{B}[\Phi, \mathbf{A}]\} \stackrel{b}{=} \langle\phi|[\mathbf{A}, \mathbf{B}]|\phi\rangle, \end{aligned}$$

where (a) follows from Lemma 5 and (b) follows from the cyclicity of trace. This completes the proof of Lemma 4.

#### J. Proof of Proposition 1.

Without loss of generality, assume  $a < b$ . Next, consider the following inequalities:

$$\begin{aligned} \mathbb{E}[\mathbf{g}(a_p, b_q)] &= \sum_{a_p \neq b_q} \frac{1}{c(c-1)} \mathbb{E}\left[\frac{c}{2}(g_{a_p} \mathbf{e}_{a_p} + g_{b_q} \mathbf{e}_{b_q})\right] \\ &= \sum_{a_p \neq b_q} \frac{1}{2(c-1)} (\mathbb{E}_{Q_{XY}}[\mathbb{E}[g_{a_p} || \phi_{x_1}\rangle, y_1]] \mathbf{e}_{a_p} + \mathbb{E}_{Q_{XY}}[\mathbb{E}[g_{b_q} || \phi_{x_2}\rangle, y_2]] \mathbf{e}_{b_q}) \\ &\stackrel{a}{=} \sum_{a_p \neq b_q} \frac{1}{2(c-1)} (\mathbb{E}_{Q_{XY}}[\nabla \mathcal{L}_{a_p}(|\phi_{x_1}\rangle, y_1)] \mathbf{e}_{a_p} + \mathbb{E}_{Q_{XY}}[\nabla \mathcal{L}_{b_q}(|\phi_{x_2}\rangle, y_2)] \mathbf{e}_{b_q}) \\ &= \sum_{a_p \neq b_q} \frac{1}{2(c-1)} (\nabla \mathcal{L}_{a_p} \mathbf{e}_{a_p} + \nabla \mathcal{L}_{b_q} \mathbf{e}_{b_q}) = \nabla \mathcal{L}, \end{aligned}$$

where (a) follows from the construction of  $g_{a_p}$  and  $g_{b_q}$ .

### K. Proof of Theorem 3.

We begin with considering Assumption 1 and using the update rule (23). Consider the following inequalities:

$$\begin{aligned}\mathcal{L}(\boldsymbol{\theta}^{(t+1)}) &\leq \mathcal{L}(\boldsymbol{\theta}^{(t)}) - \eta \nabla \mathcal{L}(\boldsymbol{\theta}^{(t)})^\top |\bar{\mathbf{Z}}^t(i, j)|^{-1} \mathbf{g}^t(i, j) + \eta^2 \frac{L_2}{2} \|\|\bar{\mathbf{Z}}^t(i, j)|^{-1} \mathbf{g}^t(i, j)\|^2 \\ &= \mathcal{L}(\boldsymbol{\theta}^{(t)}) - \frac{\beta}{(c-1)L_2} \nabla \mathcal{L}^t(i, j)^\top \left| \tilde{\mathbf{Z}}^t(i, j) - \frac{2\beta}{c} \mathbb{I} \right|^{-1} (g_i^t \mathbf{e}_i + g_j^t \mathbf{e}_j) \\ &\quad + \frac{\beta^2}{2(c-1)^2 L_2} \|\|\tilde{\mathbf{Z}}^t_{[i,j]} - (2\beta/c) \mathbb{I}_2|^{-1} [g_i^t, g_j^t]\|^2,\end{aligned}$$

where  $\nabla \mathcal{L}^t(i, j) := (\nabla \mathcal{L}_i(\boldsymbol{\theta}^{(t)}) \mathbf{e}_i + \nabla \mathcal{L}_j(\boldsymbol{\theta}^{(t)}) \mathbf{e}_j)$ . After taking the expectation of both sides with respect to  $\tilde{\mathbf{Z}}^t_{[i,j]}, g_i^t, g_j^t$  conditioned on all estimates from previous iterations, we get

$$\begin{aligned}\mathbb{E}_{(g_i^t, g_j^t, \tilde{\mathbf{Z}}^t_{[i,j]})} [\mathcal{L}(\boldsymbol{\theta}^{(t+1)})] &\leq \mathcal{L}(\boldsymbol{\theta}^{(t)}) - \underbrace{\frac{\beta}{(c-1)L_2} \sum_{i \neq j} \frac{1}{c(c-1)} \nabla \mathcal{L}^t(i, j)^\top \mathbb{E} \left[ \left| \tilde{\mathbf{Z}}^t(i, j) - \frac{2\beta}{c} \mathbb{I} \right|^{-1} (g_i^t \mathbf{e}_i + g_j^t \mathbf{e}_j) \right]}_{T_1} \\ &\quad + \underbrace{\frac{\beta^2}{2(c-1)^2 L_2} \sum_{i \neq j} \frac{1}{c(c-1)} \mathbb{E} [\|\|\tilde{\mathbf{Z}}^t_{[i,j]} - (2\beta/c) \mathbb{I}_2|^{-1} [g_i^t, g_j^t]\|^2]}_{T_2}. \quad (47)\end{aligned}$$

Now, we simplify the term  $T_2$  as:

$$T_2 \leq \sum_{i \neq j} \frac{1}{c(c-1)} \mathbb{E} [\|\|\tilde{\mathbf{Z}}^t_{[i,j]} - (2\beta/c) \mathbb{I}_2|^{-1}\|^2] \mathbb{E} [\|[g_i^t, g_j^t]\|^2] \leq \sum_{i \neq j} \frac{1}{c(c-1)} \alpha^2 = \alpha^2,$$

where the first inequality follows from the definition of the spectral norm and the fact that independent quantum samples are used to construct  $\tilde{\mathbf{Z}}^t_{[i,j]}, g_i$ , and  $g_j$ , and the second inequality follows by defining  $\alpha^2 = \max_{(i,j)} \mathbb{E} [\|\|\tilde{\mathbf{Z}}^t_{[i,j]} - (2\beta/c) \mathbb{I}_2|^{-1}\|^2] \mathbb{E} [\|[g_i^t, g_j^t]\|^2]$  and considering the following arguments. From Remark 1, there exists a  $\beta > 0$  for every  $c > 0$  such that the  $2 \times 2$  matrix  $(\tilde{\mathbf{Z}}^t_{[i,j]} - (2\beta/c) \mathbb{I}_2)$  has positive eigenvalues for all possible measurements outcomes. Moreover, given a set of measurement outcomes, the eigenvalues of this  $2 \times 2$  sub-matrix eventually saturate to a value independent of  $c$  and solely dependent on  $\beta > 0$ . This occurs because, as  $c$  increases, the diagonal entries of this  $2 \times 2$  matrix are predominantly governed by  $\beta$ . Therefore, the spectral norm of the inverse of this  $2 \times 2$  sub-matrix, i.e., the inverse of its minimum eigenvalue, is bounded. Furthermore, for a bounded loss function  $\ell(y, \hat{y})$ , the partial derivative estimators  $g_i^t$  and  $g_j^t$  are also bounded. This implies the product of the expectation of these estimators is also bounded.

On a similar note, we can rewrite  $T_1$  as:

$$\begin{aligned}
T_1 &= \sum_{i \neq j} \frac{1}{c(c-1)} \nabla \mathcal{L}^t(i, j)^\top \mathbb{E} \left[ \left| \tilde{\mathbf{Z}}^t(i, j) - \frac{2\beta}{c} \mathbb{I} \right|^{-1} \right] \nabla \mathcal{L}^t(i, j) \\
&\stackrel{a}{\geq} \sum_{i \neq j} \frac{1}{c(c-1)} \nabla \mathcal{L}^t(i, j)^\top \left( \mathbb{E} \left[ \left| \tilde{\mathbf{Z}}^t(i, j) - \frac{2\beta}{c} \mathbb{I} \right| \right] \right)^{-1} \nabla \mathcal{L}^t(i, j) \\
&\stackrel{b}{=} \sum_{i \neq j} \frac{1}{c(c-1)} \nabla \mathcal{L}(\boldsymbol{\theta}^{(t)})_{[i,j]}^\top \left( \tilde{\mathcal{F}}^t(i, j) + \frac{2\beta}{c} \mathbb{I} \right)^{-1} \nabla \mathcal{L}(\boldsymbol{\theta}^{(t)})_{[i,j]} \\
&\stackrel{c}{\geq} \left( \sum_{i \neq j} \frac{1}{c(c-1)} \nabla \mathcal{L}^t(i, j) \right)^\top \left( \sum_{i \neq j} \frac{1}{c(c-1)} \left( \tilde{\mathcal{F}}^t(i, j) + \frac{2\beta}{c} \mathbb{I} \right) \right)^{-1} \left( \sum_{i \neq j} \frac{1}{c(c-1)} \nabla \mathcal{L}^t(i, j) \right) \\
&= \frac{4}{c^2} \nabla \mathcal{L}(\boldsymbol{\theta}^{(t)})^\top \left( \frac{2}{c(c-1)} \mathcal{F}^t(\boldsymbol{\theta}) + \frac{4(c-2)}{c^2} \beta \mathbb{I} \right)^{-1} \nabla \mathcal{L}(\boldsymbol{\theta}^{(t)}) \\
&\stackrel{d}{\geq} \frac{8\bar{\mu}}{c^2} (\mathcal{L}(\boldsymbol{\theta}^{(t)}) - \mathcal{L}(\boldsymbol{\theta}^*)).
\end{aligned}$$

In the above inequalities, (a) follows because the inverse is a convex operator function over the space of positive definite operator [Nor11], (b) follows from Remark 1 and by defining  $\tilde{\mathcal{F}}^t(i, j) := \mathbb{E}[\tilde{\mathbf{Z}}^t(i, j)] - \left(\frac{4\beta}{c}\right)\mathbb{I}(i, j)$ , where  $\mathbb{I}(i, j)$  is a projection operator with all zero elements except at diagonals corresponding to coordinates  $i$  and  $j$ , (c) follows from Keifer inequality [Kie59, Lemma 3.2], and (d) follows from Assumption 2. After putting the value of  $T_1$  and  $T_2$  in (47) and taking expectation with respect to all estimates from previous iterations, we get

$$\mathbb{E}[\mathcal{L}(\boldsymbol{\theta}^{(t+1)}) - \mathcal{L}(\boldsymbol{\theta}^*)] \leq \left(1 - \frac{8\bar{\mu}\beta}{c^2(c-1)L_2}\right) \mathbb{E}[(\mathcal{L}(\boldsymbol{\theta}^{(t)}) - \mathcal{L}(\boldsymbol{\theta}^*))] + \frac{\alpha^2\beta^2}{2(c-1)^2L_2}$$

Finally, applying this inequality recursively, we get

$$\begin{aligned}
\mathbb{E}[\mathcal{L}(\boldsymbol{\theta}^{(t)}) - \mathcal{L}(\boldsymbol{\theta}^*)] &\leq \left(1 - \frac{8\bar{\mu}\beta}{c^2(c-1)L_2}\right)^t (\mathcal{L}(\boldsymbol{\theta}^{(0)}) - \mathcal{L}(\boldsymbol{\theta}^*)) + \frac{\alpha^2\beta^2}{2(c-1)^2L_2} \sum_{k=0}^{t-1} \left(1 - \frac{8\bar{\mu}}{c^2(c-1)L_2}\right)^k \\
\mathbb{E}[\mathcal{L}(\boldsymbol{\theta}^{(t)}) - \mathcal{L}(\boldsymbol{\theta}^*)] &\leq \left(1 - \frac{8\bar{\mu}\beta}{c^3L_2}\right)^t (\mathcal{L}(\boldsymbol{\theta}^{(0)}) - \mathcal{L}(\boldsymbol{\theta}^*)) + \frac{c}{8\bar{\mu}} \alpha^2\beta^2.
\end{aligned}$$

This completes the proof of Theorem 3.

## L. Supplementary Information for Section V.

**Regularization constant  $\beta$ :** We choose  $\beta$  by empirically assessing the positive definiteness of  $2 \times 2$  sub-matrix  $\tilde{\mathbf{Z}}_{[i,j]}$  for all possible cases of measurement outcomes. If  $\beta > 0.643$  for  $c = 9$ ,  $\beta > 0.572$  for  $c = 16$ ,  $\beta > 0.536$  for  $c = 30$ ,  $\beta > 0.5295$  for  $c = 36$ , and  $\beta > 0.5218$  for  $c = 48$ , we observe the sub-matrix  $\tilde{\mathbf{Z}}_{[i,j]}$  is positive definite for all possible measurement outcomes. Therefore, we chose a sufficiently small value for  $\beta$  that is close, but not too close, to the threshold.

The regularization constant  $\beta$  is a hyper-parameter to trade off numerical instabilities for the faithful E-QFIM estimation. A small  $\beta$  leads to a faster convergence, while a larger  $\beta$  aligns the update closer to the RQSGD approach. However, using a significantly small  $\beta$ , closer to the threshold, leads to large noisy oscillations in the 2-QNSCD loss function due to numerical instabilities in the inversion of  $\bar{\mathbf{Z}}_{[i,j]}$ . Figure 5 shows the 3Q Exp2 example (from Fig.4) for different values of  $\beta$  and illustrates how the different values of  $\beta$  impacts the performance of 2-QNSCD. As  $\beta$  increases, 2-QNSCD approaches the performance of 6-RQSGD and then the 2-RQSGD.

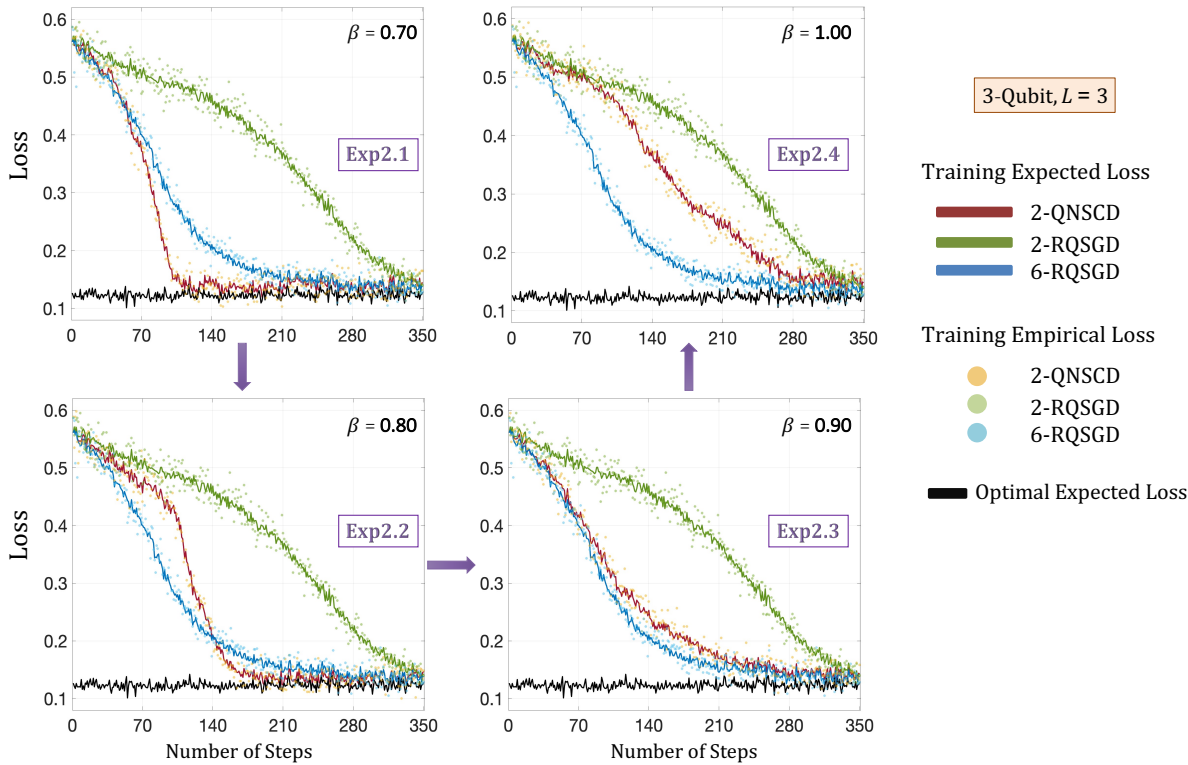


Figure 5: Performance of 2-QNSCD with 3-Qubit for different regularization constant  $\beta$ .

**PQC considered in Figure 4:** The PQC for three qubits configuration is shown below. The parameters are represented using the following convention:  $\omega_i = \theta_{(i/d, i \% d)}$ , where  $d$  is the number of qubits,  $i/d$  represents the integer (floor) division of  $i$  by  $d$ , and  $i \% d$  ( $i$  modulo  $d$ ) gives the remainder of  $i$  divided by  $d$ .

